MAPPING NUCLEAR FALLOUT USING THE WEATHER RESEARCH & FORECASTING (WRF) MODEL

THESIS

Joseph C.H. Schofield, Civilian, USAF

AFIT/CWMD/ENP/12-S01

DEPARTMENT OF THE AIR FORCE
AIR UNIVERSITY

AIR FORCE INSTITUTE OF TECHNOLOGY

Wright-Patterson Air Force Base, Ohio

AFIT/CWMD/ENP/12-S01

MAPPPING NUCLEAR FALLOUT USING THE WEATHER RESEARCH & FORECASTING (WRF) MODEL

THESIS

Presented to the Faculty

Department of Aeronautics and Astronautics

Graduate School of Engineering and Management

Air Force Institute of Technology

Air University

Air Education and Training Command

In Partial Fulfillment of the Requirements for the

Degree of Master of Science in Combating Weapons of Mass Destruction

Joseph C.H. Schofield, BS

Civilian, USAF

September 2012

AFIT/CWMD/ENP/12-S01

MAPPING NUCLEAR FALLOUT USING THE WEATHER RESEARCH & FORCASTING (WRF) MODEL

Joseph C.H. Schofield, BS
Civilian, USAF

Approved:

_____//SIGNED//_____	_____
Steven T. Fiorino, PhD (Chairman)	Date
_____//SIGNED//_____	_____
John W. McClory, PhD (Member)	Date
_____//SIGNED//_____	_____
Stephen R. McHale, LTC, USA (Member)	Date

Abstract

There are many models that attempt to predict transport & dispersion (T&D) of particulate matter in the sensible atmosphere. The majority of these existing models are unable to incorporate atmospheric processes such wet deposition through scavenging and cloud condensation nuclei (CCN) formation. To this end, the numerical weather prediction (NWP) model known as the Weather Research & Forecasting with Chemistry (WRF/Chem) Model is studied to determine its suitability as a potential tool for predicting particulate T&D following an atmospheric nuclear detonation. This is done by modifying relevant modules, originally designed to predict the settling of volcanic ash, such that a stabilized cloud of nuclear particulate is initialized within the model. This modified code is then executed for various atmospheric test explosions and the results are qualitatively and quantitatively compared to historical dose-rate contour data contained in DNA-1251-EX. The same simulations were also performed using the offline (NWP wind flow separately applied) Hazard Predication Assessment & Capability (HPAC) Model and Hybrid Single Particle Lagrangian Integrated Trajectory (HYSPLIT) Model. By comparison, using WRF/Chem for particulate tracking allows for the incorporation of important meteorological processes inline with dispersion processes and leads to more realistic fallout pattern with effects of the fallout coupled back into the numerical weather forecast.

Acknowledgments

This research would not be possible without the guidance of Dr. Steven Fiorino, to whom I owe a sincere debt of gratitude. His support and insight throughout this effort was tremendous, and certainly appreciated. I would also like to thank my entire research committee as well as my supervisor Dr. Nancy Giles for their continuous support, encouragement, and perhaps most of all, patience.

Joseph C.H. Schofield

Table of Contents

Page

List of Figures

Page

List of Tables

Page

MAPPPING NUCLEAR FALLOUT USING THE WEATHER RESEARCH & FORECASTING (WRF) MODEL

1. Introduction

1.1 Introduction

The reliability of any nuclear fallout model is intrinsically limited by the degree to which the model can accurately incorporate and predict changes in the local atmosphere. Over the past decade, the meteorological research community has developed numerical weather prediction (NWP) models that for the first time are able to account for the coupled nature of climate-chemistry-aerosol-cloud-radiation feedbacks. In particular, the incorporations of aerosol behavior and dynamic chemistry not only assimilate natural atmospheric processes previously unaccounted for, but also become particularly important in predicting how air quality affects local weather and climates. The relative contribution of coupled aerosol and chemistry feedbacks may become even more exaggerated when attempting to model the residual radiation from an atmospheric nuclear detonation, and thus the value of these new online numerical weather prediction models may be as of yet not fully realized.

Perhaps the most successful of these new models is the Weather Research & Forecasting (WRF) Model, which in 2006 was adopted as the model for the North American Mesoscale (NAM) forecast used by the National Centers for Environmental Prediction. While the coupled chemical processes handled by a WRF/Chem add-on module are not currently being evaluated within NAM forecasts (likely because of a lack of input data), researchers have successfully utilized the open-source-code WRF with Chemistry to better understand how air pollution aerosols disperse in the environment.

Such research is likely to be relevant to fallout model development, as there is currently no in-line fallout modeling platform being used by professionals at relevant government agencies. The in-line technique is important as current operational fallout models are "off-line" in that they only use the large-scale wind flow from NWP models and a separate, uncoupled turbulence model to characterize the distribution.

1.2 Background

Although there is no developed in-line and coupled fallout model, research into the potential of such models was done by Maj John Englert, who built a prototype in-line model using a modified Regional Atmospheric Modeling System (RAMS) model [1]. In his prototype, carefully chosen parameters were modified to simulate a large aerosol-type distribution of particulates following a nuclear detonation. One way in which the WRF/Chem model may improve upon the prototype model developed by Englert is that fundamental source-code parameters such as hail distributions need not be modified. The WRF/Chem code includes modules that make it relatively simple to introduce parameterized aerosol distributions into a modeled environment. This included aerosol package is highly developed and can accurately predict the dynamics of various aerosol distributions, including the effects of precipitation scavenging and the production of cloud condensation nuclei in the atmosphere.

1.3 Problem Statement

By applying the Weather Research & Forecast (WRF) weather model to problems in nuclear fallout forecasting, this research will address two fundamental questions: first, can WRF, along with its WRF/Chem module, be used to model a nuclear event, and can

such a model make better predictions than current off-line fallout modeling packages such as the Hazard Predication Assessment & Capability (HPAC) Model and the Hybrid Single Particle Lagrangian Integrated Trajectory (HYSPLIT) Model?

1.4 Motivation

The value in pursuing these questions arises from the fundamental difference between existing models and WRF w/Chem, which is that the latter has the ability to compute and predict chemical reactions and use these predictions to more realistically feedback into microphysical process predictions in the atmosphere. This ability comes from an additional family of calculation subroutines that work in-tandem with the traditional three packages of modules in NWP models that are used by HPAC and HYSPLIT: dynamics, microphysics, and radiative transfer. The addition of a fourth package accounting for chemical interactions and aerosols within the atmosphere represents a truly significant breakthrough in atmospheric modeling – not just in terms of being able to predict weather (or in this case, dynamically track radioactive particulates), but also as a step towards being able to more fully understand what is happening in the boundary layer of the atmosphere.

WRF/Chem has been designed to account for naturally occurring chemistry as part of WRF's normal weather prediction routines, with examples that include varying levels of nitrogen produced by soil, oxygen production from forests, and numerous atmospheric photolysis reactions. In addition to intrinsic natural chemical procedures that WRF/Chem provides, the module also has the ability to incorporate foreign chemical

particulate introduced into the program by the user, and this feature may prove to be especially important for developing highly accurate fallout models.

Current models use pre-detonation local atmospheric conditions and predictions to specify the transport of radioactive and other fallout particulate. However, it is well established that a real-world nuclear detonation can itself significantly modify atmospheric conditions, and thus current models may be inadequate for high-accuracy fallout predictions. If WRF/Chem can successfully illustrate how a nuclear event changes weather conditions, this "in-line" coupling of chemistry and atmospheric microphysics may well lead to the development of a next-generation fallout modeling program.

1.5 Scope

This research is designed to investigate a potential evolution in the fallout models being used by military and civilian agencies to predict fallout from a nuclear event. The scope of what this work will provide includes a direct comparison of nuclear fallout deposition predicted by HPAC to that same deposition predicted by WRF/Chem. This research will also provide a comparative analysis of the performance of WRF as a fallout model as compared to the existing models using NWP only for large-scale flow such as HPAC and HYSPLIT.

1.6 Hypothesis

This research asserts that WRF/Chem can provide a more accurate, more detailed mapping of nuclear fallout than HPAC or HYSPLIT. This will likely be due in large part to the fact that local air quality is affected to an extreme degree following a nuclear blast,

making the need for chemical-aersosol-weather numeric feedbacks for fallout models even greater than for air pollution models. The WRF/Chem predictions will not be based on a false assumption that local meteorological conditions remain smoothly continuous during a large nuclear blast and thus the model might potentially be applied to develop what could be considered the most reliable nuclear fallout model to date.

1.7 Document Structure

Chapter 2 provides context for this work by walking through the results of some previous fallout modeling research. It also provides a detailed description of what tools the WRF model uses with respect to four major elements of atmospheric modeling: microphysics, dynamics, radiative transfer, and chemistry. Chapter 3 outlines the methodology in implementing WRF/Chem with the goal of modeling fallout from a large nuclear detonation. Chapter 4 includes the results of the WRF fallout predictions and provides analysis on the accuracy and effectiveness of the implementation. This chapter also compares the results to those of HPAC and HYSPLIT. Chapter 5 provides a summary of the results of this research and makes recommendations concerning its potential usefulness as a fallout forecasting tool along. Potential for further research is also discussed.

2. Theory and Literature Review

2.1 Chapter Overview

This chapter begins with an overview of the fundamental principles of residual nuclear fallout in order to provide a theoretical context for this research. The next section includes discussion of how aerosols affect important microphysical processes within clouds. Further background and historical perspective is then developed through the detailed review of previous research concerning in-line nuclear fallout modeling, followed by consideration of currently used transport and dispersion (T&D) models, in particular those employed by the Department of Defense (DOD) and the National Oceanic and Atmospheric Administration (NOAA). An overview of the WRF Model, as well as add-on modules contained within WRF/Chem is provided followed by a brief explanation of the availability of historical meteorological data. Finally a discussion of the methods often employed to quantitatively asses the quality of a model's fallout predictions is provided.

2.2 Nuclear Fallout Fundamentals

Any nuclear detonation occurring low enough in the sensible atmosphere will result in some measurable fallout of radioactive particle onto the ground over time. The manner in which particulate is deposited onto the ground is dependent on the explosive yield of the detonation, the atmospheric height at which the detonation occurred, and the local meteorological conditions at detonation. The latter of these has proven to be the most difficult to accurately assimilate into fallout models, as the term "local meteorological conditions" refers to a myriad of special and physical parameters which

are highly dynamic and difficult to precisely measure. These conditions can also be severely affected by the detonation itself, adding to the difficulty of making accurate fallout predictions.

2.2.1 Fireball

In the first few instants following a nuclear explosion, fireball temperatures can exceed 10^7 K, and the resulting gradient between the atmospheric and the fireball temperatures will cause the fireball to rise [2]. The temperature will decrease initially through radiative cooling, but as toroidal motion of the fireball begins to dominate, entrainment of cold air will result in convective cooling. Despite these cooling processes, temperatures remain so high within the fireball that all matter will be completely vaporized and ionized (plasmized). This includes all dirt and surface debris drawn up convectively into the fireball, which for surface bursts can be as much as 0.3 actual tons of dirt per TNT-equivalent-ton yield of the weapon.

It is assumed that the plasmized matter is approximately uniformly mixed until the fireball temperature drops to a point where the highest melting-point fission fragments begin to condense. This usually occurs within about 10 seconds of the initial detonation. As the fireball continues to cool, radiochemical fractionation processes occur in which refractory fission products (i.e. those with higher melting points) condense first and eventually exist mostly within the volume of the formed particles. Volatile fission products (with lower melting points), on the other hand, condense on top of the already solid refractory particles, and thus will exist mostly within the surface area of the final formed particles [3]. This process is important to fallout modeling theory for two reasons. First, the fractionation process determines the initial stabilized particle size

distribution of the fallout. Also, the volatile or refractory nature of each fission fragment isotope determines how that isotope will ultimately contribute to fallout radioactivity doses.

2.2.2 Particle Size Distribution of Initial Stabilized Cloud

The particle size distribution of the initial stabilized cloud has been modeled by many different distributions types and combinations. Perhaps the most commonly used size distribution is represented by either a unimodal or bimodal distribution where each mode is represented by a lognormal function credited to Dr. George H. Baker and given as

$$N(r) = \frac{N_t}{\sqrt{2\pi}\beta r} e^{-\frac{1}{2}\left(\frac{\ln(r)-\alpha_0}{\beta}\right)^2} \tag{2.1}$$

where

$$N(r) = number\ of\ \ particles\ of\ \ radius\ r\ \ per\ unit\ radius$$
$$N_t = total\ number\ of\ \ particles$$
$$\alpha_0 = natural\ logarithm\ of\ \ the\ median\ radius$$
$$\beta = logarithmic\ standard\ \ deviation$$

Analysis of over 100 nuclear test explosions by Baker showed that the particle size distribution from an atmospheric nuclear detonation could best be modeled as the sum of two of these lognormal distributions.

$$N(r) = N_1(r) + N_2(r) \tag{2.2}$$

where

$$\beta_1 = \ln(2) \quad (\mu\text{m})$$
$$\alpha_{0,1} = \ln(0.1) \quad (\mu\text{m})$$

for the smaller distribution representing components from the atmosphere and from weapon itself. For the larger distribution representing soil lofted into the atmosphere during surface or near-surface bursts,

$$\beta_2 = \ln(4) \quad (\mu\text{m})$$
$$\alpha_{0,2} = \ln(0.2) \quad (\mu\text{m})$$

Baker also found that for a surface burst n_1 contributes more total particles such that $n_1 = 2.2\, n_2$ [4].

2.2.3 Moments of Particle Size Distributions

When studying the transport of solid particulate or aerosols, it is important to delineate a particle size distribution from its related particle length, area, volume, and mass distributions and understand the value of each. A particulate source such as that described above may be conventionally defined by describing the distribution of radius lengths among the particles, however a model determining how these particles will be dispersed in a given environment may require information about how mass is distributed amongst particles. Information concerning length, area, and volume distributions is generally not used by T&D models, but a brief discussion of how they are determined is useful for understanding how particle size and mass distributions can be related.

If $N(r)$ is some particle size distribution, its distribution of length can be expressed as

$$L(r) = \frac{r\,N(r)}{\int_0^\infty r\,N(r)\,dr} \tag{2.3}$$

where the denominator is described as the particle size distribution's "first moment." This length distribution can be conceptualized as all of the particles of a particular radius' contribution to the length of a chain if every particle was lined up next to each other [5]. Surface area distributions and volume distributions can be found in a similar manner:

$$S(r) = \frac{r^2 N(r)}{\int_0^\infty r^2 N(r) dr} \quad , \tag{2.4}$$

$$V(r) = \frac{r^3 N(r)}{\int_0^\infty r^3 N(r) dr} \quad . \tag{2.5}$$

as before, the denominators in each equation are conventionally described as the particle size distribution's second and third moments, respectively. If the particulate species described by the distribution is assumed to have a constant density ρ (often the convention in T&D modeling) then

$$M(r) = V(r)\rho \tag{2.6}$$

Figure 1 shows each of the distributions described above for both the unimodal air blast distribution and the bimodal surface burst distributions. The visual trend seen in how these distributions are related extends to the vast majority of general solid particulate and aerosol size distributions.

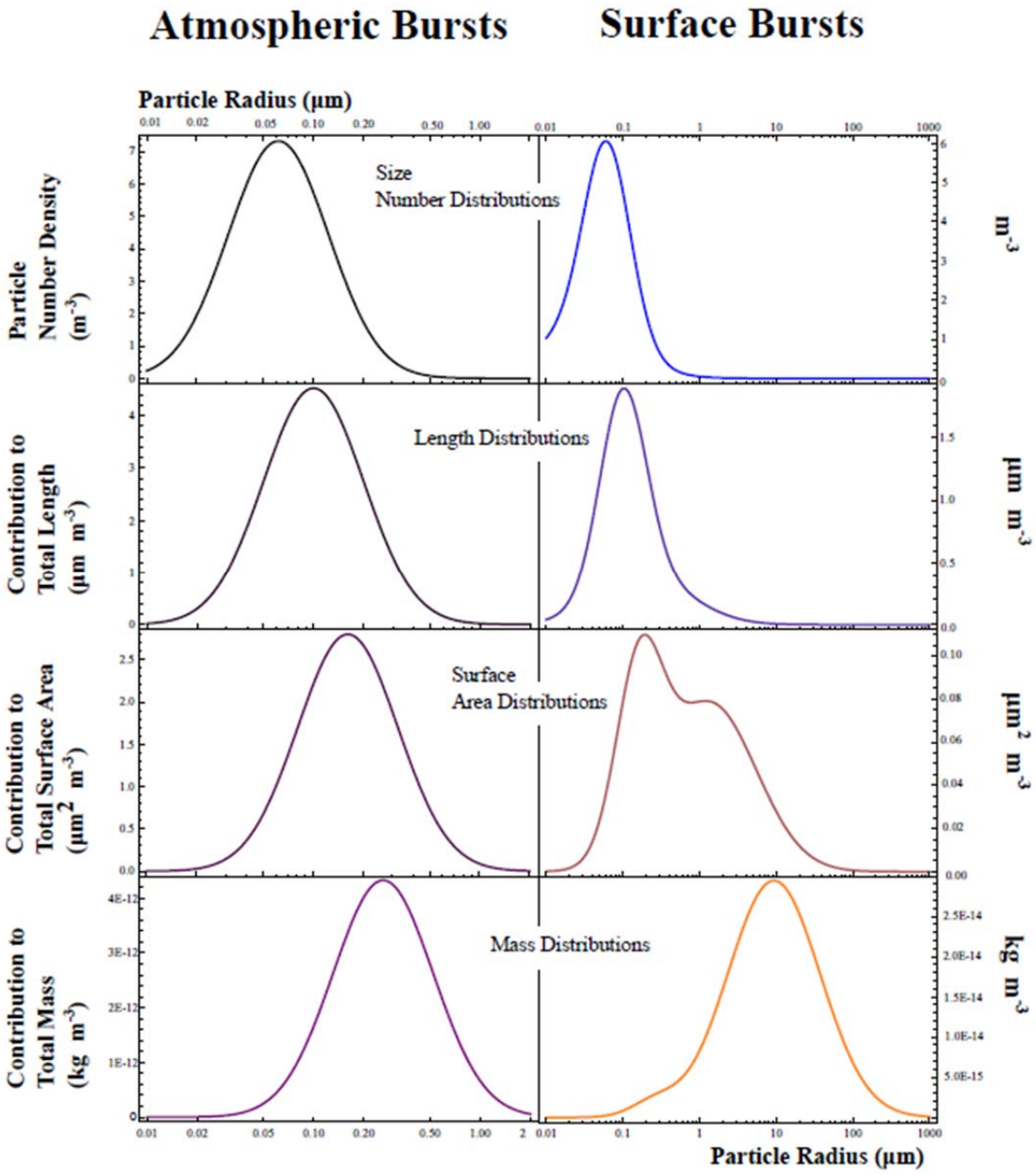

Figure 1. Particle Size Distributions for Both Atmospheric and Surface Nuclear Detonations

2.2.4 Vertical and Horizontal Profiles of Initial Stabilized Cloud

One method to quantitatively describe the vertical distribution of particles in the initial stabilized cloud is to empirically fit functions to the vertical profiles predicted by the cloud rise module in the Defense Land Fallout Interpretive Code (DELFIC). One such fit developed by Arthur Hopkins shows the relationship as

$$z_c(r,Y) = C_1 - C_2 r \tag{2.7}$$

with

$$C_1 = e^{7.889+0.34\ln Y+0.001226(\ln Y)^2-0.005227(\ln Y)^3+0.00417(\ln Y)^4}$$
$$C_2 = e^{1.574-0.01197\ln Y+0.03636(\ln Y)^2-0.0041(\ln Y)^3+0.0001965(\ln Y)^4} \quad ,$$

where

$z_c = Stabilized\ cloud\ center\ \ for\ \ particular\ \ particle\ with\ radius\ r\ [meters]$
$r = Particle\ radius\ in\ microns$
$Y = Weapon\ \ yield\ \ in\ kilotons$

[6].

A Gaussian vertical distribution about z_c is assumed with a yield and size dependent standard deviation developed by Stephen Connors, whose empirical equations also stem from analysis of DELFIC data. Conners describes a vertical thickness from top to bottom of the cloud for a particular particle size as

$$\Delta z_c(r,Y) = I_d + 2 s_d r \quad , \tag{2.8}$$

where

$$I_d = e^{7.03518+0.158914\ln Y+0.0837539(\ln Y)^2-0.0155464(\ln Y)^3+0.000862103(\ln Y)^4}$$
$$s_d = 7 - e^{1.78999-0.048249\ln Y+0.0230248(\ln Y)^2-0.00225965(\ln Y)^3+0.000161519(\ln Y)^4}$$

and where r and Y must be given in microns and kilotons, respectively and Δz_c is in meters. The standard deviation is then assumed as

$$\sigma_z = \Delta z_c / 4 \text{ [7].} \tag{2.9}$$

The horizontal center of the stabilized cloud is assumed to be at the location of detonation. It should be noted however that since external winds at low altitudes can move the cloud during stabilization, this location is only an approximation. It has been shown that the toroidal motion caused by the detonation causes the horizontal profile of the cloud to resemble a torus shape. Even though this geometry persists after stabilization time, the cloud diffuses into a Gaussian distribution at some point during its fall, and thus assuming an initial Gaussian distribution for the initial stabilized cloud is a decent approximation for modeling purposes [8] [3]. The horizontal standard deviation for this assumed horizontal Gaussian distribution can be expressed as

$$\sigma_x(Y) = \sigma_y(Y) = 1.609 e^{0.7 + \frac{\ln Y}{3} - \frac{3.25}{4+(\ln Y + 5.4)^2}} \tag{2.10}$$

where weapon yield in this case must be given in *megatons* [9].

2.2.5 Particle Settling

A method for determining the terminal fall velocities of spherical particles within a distribution was developed by Dr. Charles Bridgman, building upon empirical relationships found by Charles Norman Davies. This method does not take into account upward motion of air and other meteorological phenomenon described later in this chapter. However, discussion of this method is useful in developing an understanding of how some rudimentary nuclear fallout models predict the transport and fall times of varying particle sizes within a distribution.

Bridgman determined that for spherical particles less than roughly 10 μm in radius, stokes law for fluid motion holds reasonably valid, and as a result the fall time for each particle can be found by

$$t_a = \frac{9\int_0^{z_0} \eta(z)dz}{2r^2\rho_p g} \quad , \tag{2.11}$$

where

$$\begin{aligned} z_0 &= Particle\ height\ at\ time\ of\ \ stabilization \\ \eta &= Dynamic\ viscosity\ of\ \ air \\ r &= particle\ radius \\ \rho_p &= Density\ of\ \ the\ \ particle \\ g &= Gravitational\ acceleration \end{aligned} \tag{2.12}$$

For spherical particles of radius greater than 10 μm, a three step algorithm developed by Davies can be used to find the velocity of the of the falling particle [3] [10]. First, the quantity $R_y{}^2 C_d$ is determined, where R_y is the Reynolds number for spherical particles moving through a viscous media and C_d is the coefficient of drag. Let $Q = R_y{}^2 C_d$ and determine the quantity by

$$Q = R_y^2 C_d = \frac{32\rho_a \rho_p g r^3}{3\eta^2}. \tag{2.13}$$

Next the appropriate empirical formula below can be used to determine R_y

For $Q < 140$,

$$R_y = \frac{Q}{24} - 2.3363\times10^{-4}Q^2 + 2.0154\times10^{-6}Q^3 - 6.9105\times10^{-9}Q^4 \tag{2.14}$$

and for $100 < Q < 4.5\times10^7$,

$$R_y = 10^{-1.29536+0.986\log_{10}Q-0.046677(\log_{10}Q)^2+0.0011235(\log_{10}Q)^3} \qquad (2.15)$$

Finally, the velocity of the particle can be found by

$$v = \frac{R_y \eta}{2\rho_a r} \quad .$$

2.3 Atmospheric Feedbacks

One of the most important lessons learned from the combat detonations over Hiroshima and Nagasaki is that the local atmosphere following an atmospheric nuclear detonation is severely affected over a large area due to the particulate lofted into the atmosphere. This particulate, which can often include an amount of dirt on the order of tons, can result in cloud formation and precipitation [11]. These topics are investigated below, followed by a discussion of the techniques used to model such processes.

2.3.1 Aerosol-Cloud Interactions

Atmospheric particulate, either naturally occurring or artificially introduced, play an important role in cloud formation. As air rises, it becomes expands and cools adiabatically, a process that results in increased relative humidity. Once the saturation (100% or greater relative humidity) of the air occurs, the water soluble particulates in the atmosphere can become activated in the sense that condensation onto the particulate rapidly allows it to grow into a cloud droplet. This process is known as cloud condensation nuclei (CCN) formation and is the fundamental concept behind rain droplet formation as well as all other types of precipitation. The size distribution of the particulate in the air will influence the size distribution of the cloud droplets, which can eventually precipitate. Relatively large particulate will result in large droplets that will

likely continue to grow through collisions with other droplets within the cloud. Once the droplet reaches a certain mass, it will fall from the cloud in the form of precipitation. If an atmospheric particle size distribution has a low concentration of large particles, the probability of collisions between particles is decreased and thus precipitation is less likely to occur. Extremely small particles not collected by larger droplets often form a haze that will decrease markedly as relative humidity falls below saturation level [12].

2.3.2 Scavenging

Scavenging is the mechanism by which particulate in the air is deposited to the ground due to collision with falling precipitation. When particulate is introduced into the atmosphere, particles which escape the atmospheric boundary layer into the troposphere are able to undergo the cloud condensation nuclei (CCN) formation process described above; those that do not escape can still be scavenged to the ground during precipitation. This scavenging process is qualitatively accepted as the cause of the "black rain" observed after Hiroshima and Nagasaki combat nuclear detonations. Soot from the city-sized fires as well as traces of the radioactive fallout were scavenged to the ground by precipitation from the cumulonimbus cloud that was formed by the updrafts initiated the nuclear blast [11].

While this process comprises a critical component of nuclear weapon effects, it remains difficult to model and has been largely neglected in nuclear fallout predictions. However, multiple generic transport and dispersion (T&D) models have the ability to account for scavenging by using coefficients to represent the transfer rate of particles into raindrops. These coefficients depend largely on the size distribution and type of particulate rather than the size distribution of the raindrops [1].

2.3.3 Chemical Feedbacks

While still inside the cloud, droplets undergo aqueous chemical reactions that can result in the modification of the size distribution of the cloud aerosol such that the relative concentration of larger sized particles is increased slightly. This is known as cloud processing and has been studied by atmospheric modelers since the 1980's. A full examination of these feedbacks is beyond the scope of this research, however one well-known example highlighting their importance is an aqueous-phase oxidation reaction believed to be responsible for up to 80% of the Earth's ambient atmospheric Sulphate [13].

In the moments following an atmospheric nuclear detonation, ambient air consisting of mostly O_2 and N_2 is heated through both the central rising fireball and shock-wave compression. When these constituents are heated above 2000 K and then rapidly cooled as occurs during a nuclear detonation, the equilibrium dissociation reaction

$$N_2 + O_2 = 2NO \tag{2.16}$$

is quenched such that a high abundance of NO remains. The increased NO will result in larger production of NO_2 along with depletion of ozone through the reactions

$$NO + O_3 \rightarrow NO_2 + O_2 \tag{2.17}$$

$$NO_2 + O \rightarrow NO + O_2 \tag{2.18}$$

It is estimated that 10^{32} molecules of NO are produced per megaton of nuclear yield [11].

2.4 Previous In-Line Transport & Dispersion Modeling Research

Although there is no developed in-line nuclear fallout model, in 2005 Captain John W. Englert published research concerning the potential advantages of dispersion modeling using a modified version of the Regional Atmospheric Modeling System (RAMS) microphysics package [1]. Capt. Englert developed a prototype code by modifying parameters within the hail hydrometeor category of precipitation to match those of airborne particulate following a nuclear detonation. These modifications include changing the values for density, shape, and melting point, as well as the preventing the new category from changing phase into one of the other non-modified precipitation categories.

Given that the RAMS model incorporates cloud feedbacks from all of its hydro-categories, Capt. Englert asserted that by creating a "nuclear aerosol" category, the RAMS numerical weather prediction model is transformed into a transport & dispersion (T&D) model that can effectively account for aerosol-cloud-climate interactions. This T&D model was used as a nuclear fallout model by initializing a local volume containing the total fallout particulate at a high potential temperature in order to simulate the initial cloud rise.

Capt. Englert found that his prototype was at least somewhat effective in accounting for interactions between fallout particulate and local weather, and his results suggest that an in-line model could represent an advance in nuclear fallout prediction. One result in particular highlights both the limitations of current models and the promise of potential in-line models. By modifying the cloud material as Englert did, RAMS predicted a significant change in local rainfall, which then affected local fallout as

particulate was scavenged and deposited to the ground [1]. A fallout model in which local weather cannot be affected by particulate properties will predict certain particles as staying aloft for weeks or more, when in fact some of those particles may actually be deposited to the ground locally in a matter of hours due to induced rainfall.

2.5 Existing Fallout Models

2.5.1 DOD WMD Event Model

The Hazard Prediction Assessment Capability (HPAC) model is a widely used military tool for predicting effects on populations due to nuclear, biological, and chemical weapons and accidents. Developed by the Defense Threat Reduction Agency (DTRA), HPAC creates an initial particulate or aerosol source based on the desired weapon or accident parameters, such as yield and height of burst. HPAC then predicts the atmospheric transport of the initial source using internal terrestrial data and user provided or historical weather data. Once the model has completed transport predictions, the final step is to calculate effects on populations due to the transported material. The ability to quickly compute population effects from user defined weapon or accident scenarios helps makes HPAC the most widely used tool for the prediction of weapons of mass destruction event scenarios such as atmospheric nuclear detonations.

The most important and most computationally expensive step in the process is of course the transport prediction. The transport model used by HPAC is called the Second-order Closure Integrated Puff (SCIPUFF) model, an advanced Gaussian plume model which uses second-order turbulence techniques. Unlike the Eulerian WRF model, the SCIPUFF core is Lagrangian, meaning that the motion of particulate elements are

predicted by solving the Lagrangian equations of mass and momentum along the trajectory of a particle [14] [15]. Lagrangian methods of predicting transport are generally preferred when the emission to be tracked in from a single spatial point [16].

The meteorological input data used by SCIPUFF includes gridded two-dimensional wind vectors data, air temperature, and relative humidity for various pressure levels. Of these, the wind vector data becomes the primary driver for the transport predictions, while air temperature and humidity data help parameterize the second-order turbulent diffusion effects over a smaller scale. None of the atmospheric feedbacks described in the previous section are incorporated into the SCIPUFF model [14].

2.5.2 NOAA Transport & Dispersion Model

The Hybrid Single-Particle Lagrangian Integrated Trajectory (HYSPLIT) model was initially developed jointly by the National Oceanic and Atmospheric Administration (NOAA) and the Australian Bureau of Meteorology and was designed to serve as a complex and complete modeling system for responding to atmospheric emergencies [17] [2]. HYSPLIT is much more sensitive to the vertical atmospheric structure and incorporates vertical mixing rate gridded data into its calculations. This results in predicted deposition patterns that are clearly and visibly more complex than those for other transport and dispersion models such as HPAC.

HYSPLIT uses a hybrid of Eulerian and Lagrangian methods to predict transport and dispersion of particles, where advection and diffusion calculations are made in a Lagrangian framework, while concentration calculations are made over an Eulerian grid. First, advection of a single particle emitted from a point source is calculated by a

common and relatively simple integration method, where a particle position P at a time $t + \Delta t$ is predicted by the following algorithm: A first guess position is calculated by

$$P'(t+\Delta t) = P(t) + V(P,t)\Delta t \quad , \tag{2.19}$$

where $V(P,t)$ is three-dimensional wind velocity vector interpolated from the gridded meteorological data in both space and time. The final predicted position is found from an average of this first guess and the velocity vectors as shown in Equation 2.19.

$$P(t+\Delta t) = P(t) + \frac{V(P,t) + V(P',t+\Delta t)}{2}\Delta t \quad . \tag{2.20}$$

The time-step Δt is adaptive and varies throughout the simulation, but should always be such that the advection distance for the time-step is less than 0.75 of the meteorological grid spacing [16].

Dispersion about the path of a single particle is found by introducing a turbulent component

$$W'(t+\Delta t) = R(\Delta t)W'(t) + W''\sqrt{1-R(t)^2} + T_{LW}(1-R(\Delta t))\,\partial\sigma_W{}^2 \Big/ \partial z \tag{2.21}$$

where

$$\begin{aligned} W'(t) &= \textit{Turbulent velocity component at time } t \\ R(\Delta t) &= \textit{Time - step dependent autocorrelation coefficient} \\ W'' &= \textit{Computer - generated random component} \\ T_{LW} &= \textit{Lagrangian time scale} \\ \sigma_W &= \textit{Standard deviation of } W' \\ z &= \textit{Altitude} \quad . \end{aligned}$$

The standard deviation is calculated as

$$\sigma_W = \sqrt{\frac{K_z}{T_{LW}}} \tag{2.22}$$

where K_z is the pollutant vertical mixing coefficient calculated from meteorological variables contained in the gridded data. Positions of dispersed particles about the mean position due to advection of the wind is

$$Z(t+\Delta t) = P(t+\Delta t) + W'(t+\Delta t)\Delta t \quad [16]. \tag{2.23}$$

Deposition to the ground is calculated by HYSPLIT with both dry and wet processes being taken into account. The total deposition over a given time-step is computed using inverse time constants as

$$D_{\text{wet+dry}} = m(1 - e^{-\Delta t(\beta_{\text{dry}} + \beta_{\text{bel}} + \beta_{\text{inc}} + \beta_{\text{gas}})}) \tag{2.24}$$

where

$$\begin{aligned} m &= \textit{Pollutant mass} \\ \beta_{\text{dry}} &= \textit{Dry removal constant} \\ \beta_{\text{inc}} &= \textit{Removal constant for pollutant ingested into clouds} \\ \beta_{\text{bel}} &= \textit{Removal constant for fallining rain through particulate} \\ \beta_{\text{gas}} &= \textit{Removal constant for gases} \quad . \end{aligned}$$

The mass of the particulate is reduced by the deposited mass at each time step. The dry removal constant is calculated simply from a user-defined fall velocity v and the depth of the surface layer Δz,

$$\beta_{\text{dry}} = v / \Delta z \quad . \tag{2.25}$$

The wet removal of particulate being ingested into clouds in the boundary layer is found by

$$\beta_{inc} = \frac{F^t F_b S_r P}{\Delta z} \tag{2.26}$$

where

F^t = *Fraction of pollutant layer above tope of cloud*
F_b = *Fraction of pollutant layer above bottom of cloud*
S_r = *Average scavenging ratio by volume*
P = *Precipitation rate*
Δz_p = *Depth of pollutant layer*

Below-cloud removal from scavenging rain droplets is computed using a scavenging coefficient S_c,

$$\beta_{\text{bel}} = S_c(1.0 - F_b) \quad . \tag{2.27}$$

β_{gas} is found only for simulations involving transport & dispersion of gases and is thus zero for all solid-particulate transport & dispersion simulations [16].

2.5.3 Other Nuclear Fallout Models

Other existing fallout models range from relatively academic activity smearing algorithms to highly-developed and complex codes. Examples of the most powerful of these include the Defense Land Fallout Interpretive Code (DELFIC) developed by Army, Naval, and private laboratories, and a robust fallout deposition code (FDC) developed by Major Buck O'Day in 2009 [18] [19]. These models have many advantages over HPAC and HYSPLIT and often score better when comparing against physical nuclear test data, however this research will compare the developed model against HPAC and HYSPLIT because those two models are currently being used by military and civilian agencies as operational emergency planning tools, thus highlighting the potential for improvement in the tools that emergency planners rely on. For further information on the quality of fallout prediction amongst all of these models, the reader is referred to the Master's thesis of Major April Miller [2].

2.6 WRF Model Description

The Weather Research & Forecasting (WRF) Model was first released in 2000 with the goal of becoming a next-generation numerical weather prediction (NWP) model that could be used in both operational and research settings. The WRF model was built upon the MM5 model, which was used primarily as a research tool and whose origins can be traced back to hurricane research done by Rick Anthes in the 1960's [20]. In 2006, WRF was adopted as the North American Mesoscale (NAM) model used by the United States National Weather Service. WRF has been adopted as the national weather forecast model for many other countries around the world. It is an open-source model and is developed and maintained by numerous academic and government agencies.

As mentioned previously, certain meteorological effects of atmospheric nuclear weapon detonations are currently unaccounted for in models such as HPAC. Given the potential magnitude of their effect upon transport and dispersion of fallout particulate, they represent perhaps the most severe limitations of such models. The WRF model, along with modules from WRF/Chem are able to account for these feedbacks, incorporating their effects into each step of the numerical weather forecast in an in-line manner.

2.6.1 Key Features

The Weather Research & Forecasting (WRF) Model allows the user to define any sized resolution from micro-scale to global. It is capable of assimilating data from multiple observation and forecast formats including GFS, NOGAPS, ACARS, RAOBS, and NMC surface data, among others. WRF supports one-way, two-way and moving domain nesting with a unique output being produced for each domain. The model can be

built onto a single machine or can be compiled to run in parallel [21]. Unlike most transport & dispersion models, WRF, along with its associated extra chemistry modules that enable T&D calculations, is an Eulerian model, meaning that mass concentration of particulate elements are calculated as a function of space and time [15].

2.6.2 Numerical Methods

At each time step, the Weather Research & Forecasting Model solves the fully compressible, non-hydrostatic equations. One implication of excluding the hydrostatic assumption is that vertical advection is allowed, which when combined with microphysics modules gives the WRF model the power to predict cloud-aerosol-climate feedbacks. The exclusion of the hydrostatic equation also results in a more computationally expensive scheme, as implicit finite differencing methods must be employed. In the case of WRF, a split-explicit finite-differencing method is used in which a 3^{rd} order backwards-difference implicit scheme is used to numerically approximate vertical advection, while a 5^{th} order forward-backward explicit scheme can be used to approximate horizontal advection. This ensures that the implicit scheme is used only when necessary, thus saving computational power. The user may manipulate the horizontal advection to be between 2^{nd} and 6^{th} order [22].

WRF uses a Runge-Kutta 3^{rd} order (RK3) time marching scheme to numerically integrate the full system of governing equations at each time step. The user does have the option to use Runge-Kutta 2^{nd} order (RK2) integration, however this will only result in a stable scheme if 5^{th} or 3^{rd} order horizontal advection approximations are used. The basic algorithm for the RK3 method used by default is as follows:

Let Φ be the prognostic variables and let R(Φ) be a function representing the governing equations within the model. To find $\Phi_{t+\Delta t}$ from Φ_t ,

$$\Phi_* = \Phi_t + \frac{\Delta t}{3} R(\Phi_t) \tag{2.28}$$

$$\Phi_{**} = \Phi_t + \frac{\Delta t}{2} R(\Phi_*) \tag{2.29}$$

$$\Phi_{t+\Delta t} = \Phi_t + R(\Phi_{**})\Delta t \tag{2.30}$$

For non-linear equations, this scheme is 2nd order accurate and thus it does not represent a pure Runge-Kutta Scheme. The implementation of this scheme is based off research done by Wicker and Skamarock in 2002 [23].

2.6.3 WRF/Chem Chemical Predictions

WRF/Chem has been designed to account for naturally occurring chemistry as part of WRF's normal weather prediction routines, with examples that include varying levels of nitrogen produced by soil, oxygen production from forests, and numerous atmospheric photolysis reactions. In addition to intrinsic natural chemical procedures that WRF/Chem provides, the module also has the ability to incorporate foreign chemical particulate introduced into the program by the user, and this feature may prove to be especially important for developing highly accurate fallout models.

WRF/Chem is currently lacking in the ability to predict the kinds of radiochemical processes that occur moments after a nuclear detonation. Such processes would include the decay chains of fission products as well as the fractionation process described earlier. The incorporation of such processes is beyond the scope of this

research, and thus the initial conditions will be set at the time of cloud stabilization described previously.

2.6.4 WRF/Chem Aerosol Module

The Weather Research & Forecasting with Chemistry (WRF/Chem) model includes 3 primary modules that can be employed for modeling aerosol or particulate transport & dispersion (T&D). The most simple is named Model for Simulating Aerosol Interactions and Chemistry (MOSAIC) and defines the size distribution of the introduced aerosol in a sectional manner using size bins. The second is called the Modal Aerosol Dynamics Model for Europe & Secondary Organic Aerosol Model (MADE-SORGAM) and defines an aerosol size distribution using a modal approach. The last is a relatively new module named Goddard Chemistry Aerosol Radiation and Transport Modal (GOCART), which is able to perform simple chemistry predictions for bulk aerosol releases. Given that a modal approach is the logical choice for defining the nuclear weapons fallout particulate described earlier in this chapter, the MADE-SORGAM module will be modified and used for this research.

The core of the MADE-SORGAM module is the Modal Aerosol Dynamics Model for Europe (MADE), which is based of the Regional Particulate Model (RPM) developed by Binkowski and Shankar in 1995. Particles are assumed to be spherical and each mode within the aerosol size distribution is assumed to be lognormal with user defined mean and standard deviation, as is the case with the Baker distribution described earlier. The aerosol dynamics calculations are made inline with the atmospheric and chemistry predictions being made by WRF/Chem. The module has been designed to account for secondary particle formation, condensation, coagulation due to

Brownian motion, dry deposition, and chemistry related to sulfate, nitrate, ammonium, and water components within the aerosol.

2.7 Meteorological Data

The historical meteorological data to be employed by all three models in this research come from a joint project by The National Centers for Environmental Prediction (NCEP) and The National Center for Atmospheric Research (NCAR) called The NCEP/NCAR 40-Year Reanalysis Project. The goal of this project was to provide high-quality historic weather information for the years of 1957 through 1996 in a modern format suitable for universal employment in a wide array of numerical weather prediction models. The joint project was later able to extend the available data back through the year 1948. The data was assembled by extrapolating from a wide variety of historical raw data sources including land surface measurements, ship measurements, aircraft measurements weather balloon measurements taken by atmospheric instruments known as radiosondes, and ground observations of weather balloons known as pibal measurements [24].

The geographical span of the data is global and the horizontal resolution is about 210 km, which today is considered low-resolution weather data. It should be noted however that a significant result of the research of Major April Miller in 2011 was to demonstrate the suitability of low-resolution weather data to achieve highly realistic fallout pattern predictions [2]. A wide array of products from the 40-Year Reanalysis Project are available for download through the Computational & Information Systems

Laboratory (CISL) Research Data Archive website, though distribution is limited to government and academic communities.

2.8 Quantitative Verification of Fallout Predictions

A method of quantifying the validity of transport & dispersion predictions was developed by Warner et al., who's two-dimensional measure of effectiveness (MOE) quantity can provide significant insight into the strengths and weaknesses of a model [25]. Any fallout prediction can be compared to a known, measured set of control data using Warner's et al. method, but because actual data concerning expansive fallout from nuclear detonations is limited to government-released documents from the eras of nuclear weapons testing, evaluating any particular fallout model is only truly possible for the non-urban environments in which the tests were made, and further highlights the need for strong historical weather data as described in the previous section.

Measure of effectiveness calculations are based off three two-dimensional areas: the area in which the model correctly predicted that fallout would deposit when compared to the control measurements (area of overlap), the area in which fallout was predicted but not present in the field measurements (area of false-positive), and the area in which fallout was not predicted but was measured (area of false-negative). These values are used to determine the measure of effectiveness as

$$\begin{aligned} \mathrm{MOE} = (x, y) &= \left(\frac{A_{\mathrm{OV}}}{A_{\mathrm{OB}}}, \frac{A_{\mathrm{OV}}}{A_{\mathrm{PR}}} \right) \\ &= \left(1 - \frac{A_{\mathrm{FN}}}{A_{\mathrm{OB}}}, 1 - \frac{A_{\mathrm{FP}}}{A_{\mathrm{PR}}} \right) \quad , \end{aligned} \tag{2.31}$$

where

$$A_{OV} = Area\ of\ overlap$$
$$A_{FN} = Area\ of\ false\text{-}negative$$
$$A_{FP} = Area\ of\ false\text{-}positive$$
$$A_{OB} = Area\ of\ observation$$
$$A_{PR} = Area\ of\ prediction \quad .$$

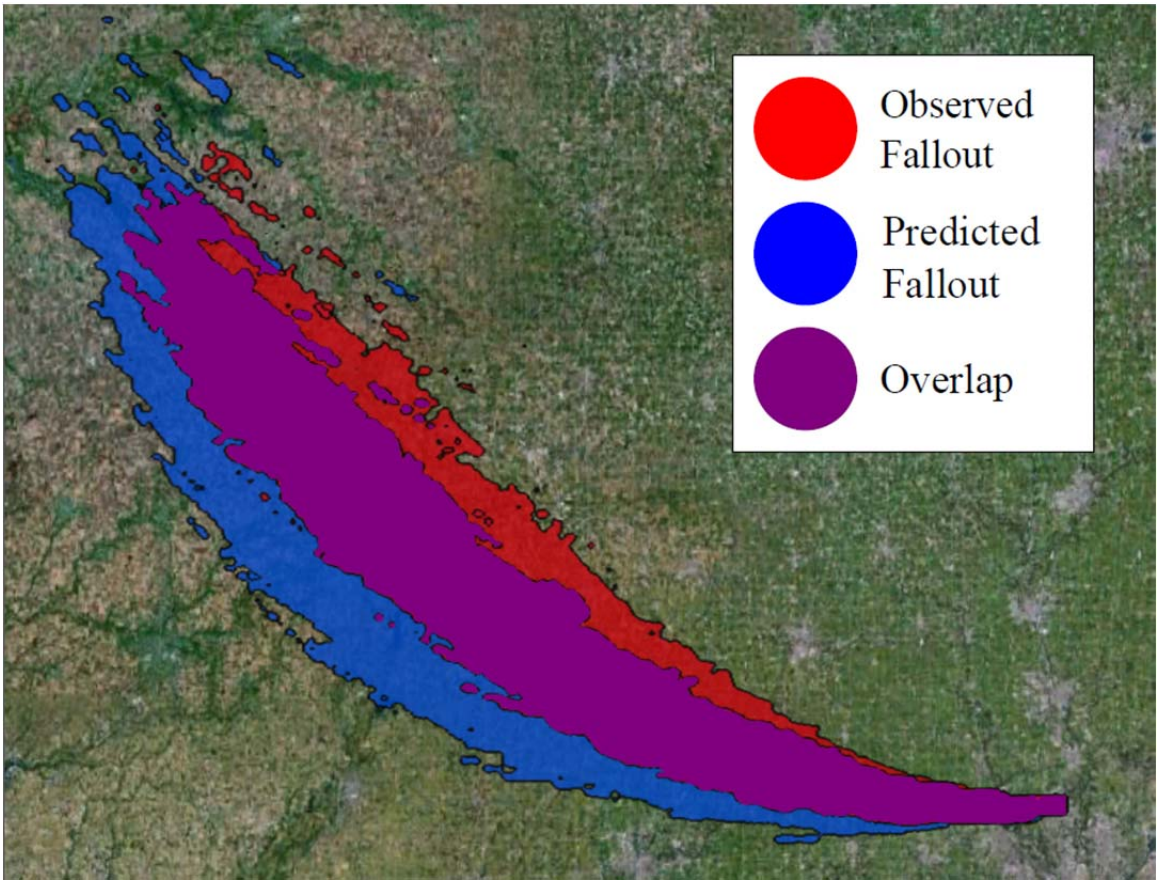

Figure 2. Hypothetical Predicted Fallout Data Shown with Control Observational Data. Areas of Non-Overlapping Blue and Red are Equivalent to Area of False-Positive and Area of False-Negative, Respectively.

Note that x corresponds to one minus the fraction of false-negative and y corresponds to one minus the fraction of false-positive. The determined MOE coordinate can be plotted on so-called 2D MOE space shown in Figure 3 along with some basic instruction

on a MOE score is interpreted. A MOE score of (0, 0) would mean that the model completely failed to predict even the basic direction of the fallout pattern, while a MOE score of (1, 1) would mean that the model data matches exactly with those of the measured control. Figure 4 illustrates how multiple models that have $x \approx y$ can be easily put in order in terms of which are more accurate and thus more desirable as a planning tool. For models who's MOE scores typically have very different x and y, it is more difficult to determine which amongst them are "better," however it is worth noting that for the purposes of emergency planning, a model that over-predicts may be more desirable than one that under-predicts.

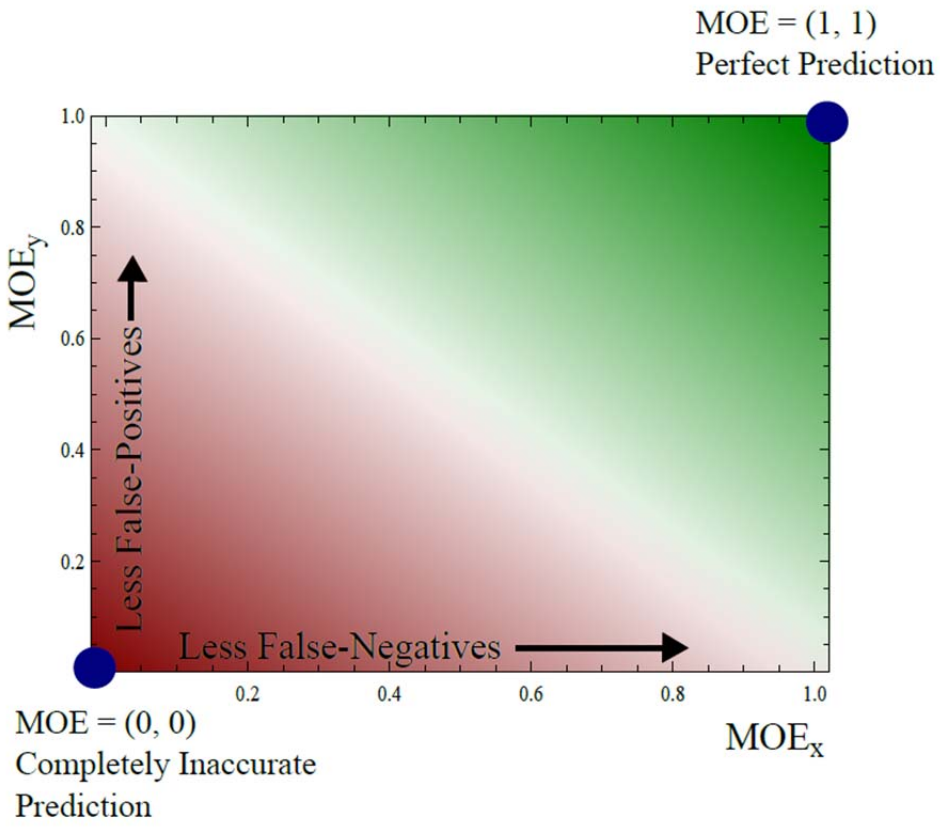

Figure 3. Two-Dimensional MOE Space. More Desirable Scores Will Exist in the Green Space While Less Desirable Scores Exist in the Red Space

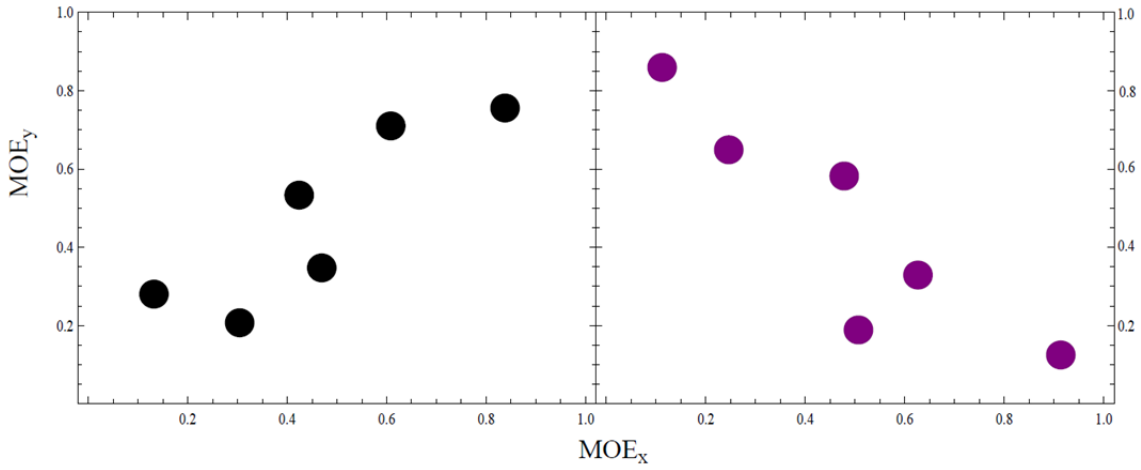

Figure 4. Two Hypothetical Sets of MOE Scores From Six Different Models. In the Case of the Left Set, The Models Can Be Ranked Clearly in Order of Desirability while in the case of the Right Set the Relative Desirability of the Models is Unclear.

When interpretation of a fallout prediction in terms of false-positives and false-negatives is not required, and the goal is to quickly score the accuracy of any particular model, Wigner et al. developed a normalized absolute difference (NAD) equation which represents a statistical measure of the "scatter" between predicted and observed fallout [25]. The equation can be represented in terms of the areas discussed previously, or as a function of the MOE coordinates.

$$\begin{aligned} \mathrm{NAD} &= \frac{A_{\mathrm{FN}} + A_{\mathrm{FP}}}{2A_{\mathrm{OV}} + A_{\mathrm{FN}} + A_{\mathrm{FP}}} \\ &= \frac{x + y - 2xy}{x + y} \quad . \end{aligned} \tag{2.32}$$

It is important to note that unlike in MOE space, a lower the NAD score suggests a more accurate model, with a NAD score of 1 representing a completely inaccurate prediction.

3. Methodology

3.1 Methodology Overview

For this research, WRF/Chem version 3.4 was used to study the transport and dispersion of a particulate source representing an initial stabilized cloud after an atmospheric nuclear detonation. This chapter will present the methods used to employ the model in such a fashion as to enable analytical comparisons with other transport and dispersion (T&D) models. Section 3.2 will describe the physical scenario that is attempt modeled with both WRF/Chem and other T&D models while Section 3.3 walks through all of the code modifications made within WRF/Chem to achieve the desired simulation. The next section will provide an overview of the procedure to execute the model, and finally Sections 3.5 and 3.6 summarizes the comparison simulations made in HPAC and HYSPLIT, respectively.

3.2 Scenario Description

All three models are evaluated by comparing results to data contained in DNA-1251-1-EX, an unclassified compilation of fallout data from test nuclear detonations at the Nevada Test Site released by the Defense Nuclear Agency in 1979. Three test shots are chosen based on availability of off-site data, which was collected by a variety of sources and methods. For the first two test-shots, Operation Tumbler-Snapper: George and Operation Teapot: Zucchini, the off-site dose-rate data are based on ground-mobile monitor measurements taken by the Radiological Safety Organization. For Operation Pumbbob: Smoky, data was compiled by The Test Manager's Committee for the

Evaluation of Radiation Doses based off ground and aerial measurements, as well as actual decay data obtained by the UCLA School of Medicine Atomic Energy Project.

Table 1. DNA 1251-1-EX Selected Test Data

Operation:	Date:	Location (lat, lon):	Yield (KT):	Height-of-Burst (ft.):
Tumbler-Snapper: George	June 1, 1952 11:55Z	(37.0481°, -116.0211°)	15	300
Teapot: Zucchini	May 15, 1955 12:00Z	(37.0947°, -116.0238°)	28	500
Pumbbob: Smoky	August 31, 1957 12:30Z	(37.1872°, -116.0678°)	44	700

3.3 Modification of Code

3.3.1 Defining Fallout Particulate

A volcanic-ash module contained within WRF/Chem v3.4 was used to simulate the initial stabilized particulate cloud. A FORTRAN module "volc_emissions.f90" was modified to move the locations of three real world volcanoes to the locations of the three nuclear test shots to be used. Within the same module, the height of the volcano was effectively changed to zero by modifying the elevation of the summit to reflect the altitude of those new locations within the Nevada Test Site. A parameter that controls how high the above the vent of the volcano ash particulate is lofted was used to define the altitude of the stabilized cloud associated with each test.

Definitions of ash particle size distributions are contained in "module_vash_settling.F.". These distributions are defined in terms of ten bins spread over a total range of 0 - 500 μm. An examination of the lognormal distributions used for

fallout particulate discussed in chapter 2 reveals that these ranges are far too large to be appropriately applied to atmospheric burst type particle size distributions. This is illustrated easily by the fact the 99.99% of the particles in the distribution have radii of less than 1.32 μm, a particle size which is still contained in the first bin for the unmodified code. Furthermore, 99.99% of the total mass of the entirety of the fallout comes from particles whose radii are less than 5.57 μm.

New bin ranges for each burst type are determined so that each bin contains 10% of the total particulate mass for that particular distribution and modified Fortran files are saved for each type. While the vast majority of total particles in the distributions will be contained in the first bin, it is more important total particulate mass be evenly distributed across the ranges since mass is much more valuable for ultimately determining the radioactivity deposited on the ground. For the smaller, atmospheric-type particle size distribution, these new bin values were found by numerically solving the iterative process described below.

Let $x_0 = 0$ and $N_t = 1$.

$$\int_{x_{n-1}}^{x_n} \frac{N_t}{\sqrt{2\pi}\,\ln(2)\,r}\, e^{-0.5\left(\frac{\ln(r)-\ln(0.1)}{\ln(2)}\right)} dr \;=\; 0.1 \qquad (3.1)$$

Solve for x_n.

For the larger, surface burst distributions bin ranges are determined from those used by the DELFIC model, which contains 100 bins based off a radioactivity distribution closely related to the mass distribution defined in Chapter 2. The ranges

taken from DELFIC are numerically verified as containing almost 10% of the mass of the particulate defined for use within the modified WRF code within 3 orders of magnitude. Both particulate mass distributions are shown in Figure 5 along with their determined bin limits. The particle size distributions' upper most limits, chosen to bound virtually 100% of particulate mass below, are not shown.

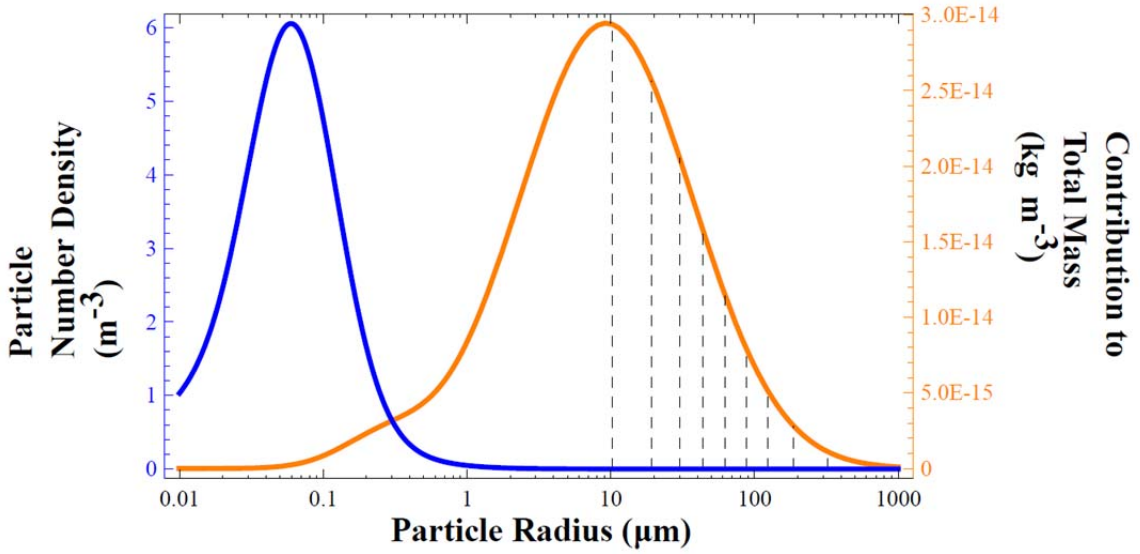

Figure 5. Particle Size Distribution and Mass Distribution Shown With Determined Size Bins

The emissions conversion module within the original code defines a total mass of injected particulate based off the volcano-type and height of injection. This was modified such that a total mass of nuclear particulate was hard coded for each simulation. The values used for these modified total masses were based off research conducted by R&D Associates. [26].

3.3.2 Other Considerations

Once the size distribution within the volcanic ash code is modified, the settling routines within the module, which include fall-velocity calculations based on Stokes' Law for fluid motion, are no longer appropriate as they result in unrealistic settling velocities and scant long-distance fallout. As discussed in Chapter 2, Bridgman asserted that for larger particles a settling velocity for falling particulate can be found from the algorithm developed by Davies [3]. Because location-dependent meteorological variables needed by Davies' algorithm are calculated by the model and during any simulation, they can be easily extracted and used within the settling routine. Thus it becomes a relatively simple task to implement Davies' algorithm into the settling module. This results in much more realistic fallout patterns.

Another modification stems from the fact that the model was originally intended to predict fallout of ash following a volcanic event. While this provides many advantages, including the fact that toroidal cloud formation code is already developed within the code and makes upwind deposition possible, one drawback is that the initial cloud is developed such that particulate is spread over a greater area than would be realistic for an atmospheric nuclear detonation with weapon yields in the tens of kilotons. Efforts to hard code initial cloud volumes were unsuccessful, and thus two other modifications were employed to combat this problem. First, the initial volumes for all ten particle sizes were reduced by a factor of 0.01. This was done within the emissions conversion module. Second, a "volcanic correction factor" was introduced to the final dose-rate conversion so that the initial spread of activity is concentrated over a much smaller area than the model would otherwise suggest.

3.4 WRF/Chem Deposition Simulation

3.4.1 WRF Preprocessing

To create the initial source definition, an add-on executable program referred to as prep_chem_sources v1.2 must be run. This program must be configured and compiled manually and it is important to note that any modifications to code such as those described above must be made before compilation of the executable. In other words, if one wishes to make small changes to the code, recompiling the executable is required for those changes to take effect. Using a preassembled text file, emission types and options are specified by the user. In the case of this research, a modified volcanic source is selected and parameters such as total mass, elevation of injection, and time-length of injection are specified. Three minute injection duration is chosen to represent the general time of cloud stabilization and to ensure that the entire particulate mass is lofted into the atmosphere very quickly relative to the time-step of the model. Once parameters are defined, the executable is run and a volcanic emission file is generated to be used later on in the WRF/Chem execution process.

Before any WRF run is executed (with or without chemistry), the WRF preprocessing system (WPS) must be utilized to compile terrestrial and meteorological into files that can then be read by the final WRF executable. First, either a single domain or multiple nested domains are defined by the user in terms of location (latitude & longitude), size, and the spacing of the grid that WRF will make its numerical predictions on. The executable geogrid.exe can then interpolate terrestrial data (downloaded from the WRF-ARW webpage) onto user defined domains and produce terrestrial files in netCDF format.

The next step in the preprocessing sequence is to the link in any meteorological data that is to be used for initial and boundary conditions of the model. A UNIX shell script included with WRF links in the desired data and renames them to a form that the executable ungrib.exe expects. That program takes the linked in files (in GRIB1 or GRIB2 file format) and converts them into an intermediate format used only by the WPS. It is important to note that the correct variable table, which is always called "Vtable", must be present in the WPS directory when ungrib.exe is run. Variable tables for many common meteorological analysis and forecast data (NAM, GFS, NOGAPS, etc.) are provided in a subdirectory. The data for this research is from The NCEP/NCAR 40-Year Reanalysis Project (NNRP) described in Chapter 2. The products needed for use with WRF's NNRP variable table are 6-hour intervals of gridded analysis data for a wide assortment of variables on 18 pressure levels, and 6-hour intervals of two dimensional forecast surface data. The final step when utilizing the WPS is to run metgrid.exe, which takes the intermediate meteorological data file and horizontally interpolates it onto the generated domain. The output of this executable is a netCDF file which effectively serves as the input for WRF.

3.4.2 Running WRF/Chem

After preprocessing, running WRF generally has two steps, the first being the execution of real.exe, which vertically interpolates the data from the WPS and creates actual initial and boundary condition files, and the second being the execution of wrf.exe, which generates the forecast. However, the process becomes more complex when attempting to run WRF with chemistry, or specifically in the case of this research, WRF with volcanic ash. The volcanic emissions file generated by prep_chem_sources is

moved to the WRF execution directory and renamed volc_d01. The file real.exe is then run with the "chemistry option" turned off (this and all other options are specified in the file namelist.input). As previously described, this generates the ultimate initial and boundary conditions for the model. After changing the chemistry option from "chemistry off" to "volcanic ash settling," a program convert_emiss.exe is executed. This utilizes those conditions and brings in the volcanic emissions file to generate an emissions file that WRF/Chem can understand. The initial and boundary conditions files are written to the files wrfinput_d01 and wrfbdy_d01 respectively, and the former must be saved from being overwritten by renaming it wrfinput_d01.SAVE (note that the .SAVE is arbitrary). With the chemistry option still set for volcanic ash, real.exe is run once more and again a file named wrfinput_d01 is generated, however, this file contains the ultimate information concerning the ash emission. This file is renamed to wrfchemi_00z_d01 and the saved input conditions file is renamed back to wrfinput_d01. Note that were emissions to be injected continuously, as is the case with general air quality modeling, the wrfchemi_XXz_d01 type files would need to be generated for every twelve hours. Finally, with chemistry still turned on wrf.exe can be executed with boundary, initial, and emissions conditions being employed by the program.

3.4.3 Extracting Results

After a WRF/Chem simulation is executed, an output file is generated for each model domain. These outputs are in NetCDF form and require the writing of a command script in NCAR Command Language (NCL) in order to view the desired predictions. These output files are very large and contain prediction quantities for a plethora of meteorological parameters including temperature, radar reflectivity, wind vectors,

deposition of particulate, and rainfall amongst many others. The prediction quantities that will be extracted and plotted for this research are for deposition of a modified volcanic ash source and accumulated rainfall.

3.5 HPAC Deposition Simulations

An HPAC simulation was made for each of the test shots for comparison purposes. Because HPAC requires meteorological data to be in its own proprietary format, it is not possible to use the NCAR/NCEP 40-Year Reanalysis data in its original GRIB format. As part of his Master's research, Kevin Pace developed a Fortran routine that when combined with a NOAA-built executable called wbrib.exe, can be used to extract to appropriate variables, namely two-dimensional wind vectors, and parse the data into a .prf file suitable for use in HPAC [27]. Using Pace's routine, .prf files were created for each of the test shots studied in this research. Because HPAC has the ability to create a particulate source based on the weapon scenario input by the user, there is relatively little needed to be done by the user other than to provide location, weapon yield, and height-of-burst along with the meteorological data mentioned above. The terrain option in HPAC was changed to its desert preset and the humidity option was set to dry. Spatial domains were adjusted so that all of the expected fallout would be present within them.

3.6 HYSPLIT Deposition Simulations

The general methodology for HYSPLIT comparison simulations follows from the research of Major April Miller [2] with some deviations. As reported by Miller, HYSPLIT has the ability to download any requested data from the NCEP/NCAR 40-Year

Reanalysis Project in a format already suitable for the program and thus no conversion of meteorological data is required. One of the major limitations of HYSPLIT is that the model releases all emissions from one or multiple point sources, making its ability to model the dispersion of a large homogenous source, such as a stabilized nuclear cloud, limited. However, multiple point sources can be distributed in such a way that such large sources can be at least somewhat more effectively modeled. HYSPLIT automatically and evenly distributes the total injected particulate or aerosol source into each point source

Miller used two point sources at the top and bottom of a particular particle size's vertical profile within the initial stabilized cloud at altitudes represented as

$$\begin{aligned} z_{top} &= z_c + 3\sigma_z \\ z_{bottom} &= z_c - 3\sigma_z \end{aligned} \quad , \tag{3.2}$$

where the cloud center, z_c and standard deviation σ_z come from Conner's equations discussed in Chapter 2. These values were computed for each of twenty particle size groups, and because all species, or groups in HYSPLIT must be injected from the same initial point sources, a separate simulation was required for each particle size group, with the results being summed together afterwards.

For this research, ten points-source locations and ten particle size groups are used, with those size groups being the same as those used for the WRF simulations described in a previous section in this chapter and shown in Figure 5. The top and bottom of a particle group's vertical distribution is represented as

$$\begin{aligned} z_{top} &= z_c + 2.5\sigma_z \\ z_{bottom} &= z_c - 2.5\sigma_z \end{aligned} \quad . \tag{3.3}$$

Five of the ten points are placed along the vertical line connecting z_{top} and z_{bottom} (from Equation 3.3) at altitudes z_c, $z_c \pm \sigma_z$, and $z_c \pm 2.5\sigma_z$. In an attempt to have the horizontal distribution of the stabilized nuclear cloud taken into account by the model, four injection points are chosen such that if the horizontal coordinates of the center of the cloud is $z_c = (z_{cx}\ ,\ z_{cy})$, then these new point sources are $(z_{cx}\ \pm\ 2.5\sigma_x\ ,\ z_{cy})$ and $(z_{cx}\ ,\ z_{cy}\ \pm\ 2.5\sigma_x)$ where σ_x comes from Pugh and Galiano's relationship discussed in Chapter 2. This distribution of points reflects the "pancake" nature of the stabilized clouds following most nuclear detonations. One additional point source is placed directly underneath z_c, at an altitude of $z_{bottom}/2$. This point-source injects 10% of the total particulate and accounts for the stem of fallout particulate underneath the cloud following most atmospheric detonations.

Unlike in Miller's research, the locations of the point sources were not defined for each particle size group. The groups are broken up into light and heavy particle groups, with the seven smallest groups being considered light and the three largest being considered heavy. The ten locations described above were calculated for each of the ten groups, but only a light particle simulation and a heavy particle simulation is run, with ten locations based off the fifth smallest particle group being used as the emission point sources for the light particle simulation, and emission locations based off the second heaviest particle group were used for the heavy particle simulation. The emission points for the Teapot: Zucchini test-shot simulation can be seen in Figure 6. The results of both simulations are summed and included in the final results.

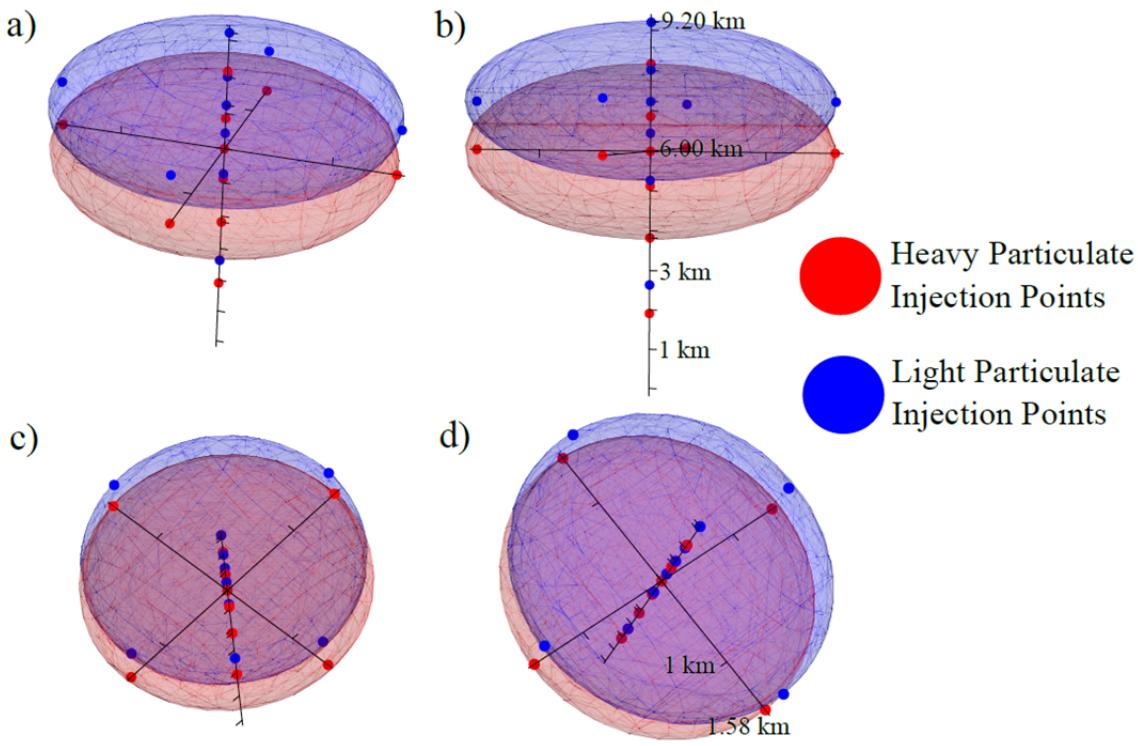

Figure 6. Emission Point Locations for Operation Teapot: Zucchini Test Shot HYSPLIT Simulation from Various Spatial Perspectives: A. Just above clouds. B. Straight ahead of heavy particle cloud center. C. From below. D. From above. Cloud surfaces illustrated to show typical "pancake" shape

Even though emission point locations are based off calculations from just one particle group within each simulation, each group is of course defined and incorporated into the HYSPLIT simulations. Amongst other parameters that can be defined for each group, the most important are particle mass density, diameter and fall speed. Density was set to $2.5\,{}^{g}\!/_{cc} = 2500\,{}^{kg}\!/_{m^3}$ for all particle groups in all simulations. The groups' diameters are chosen to be that representing the center of each size bin and the fall speeds are calculated and defined as the terminal velocity for that particular particle size. These velocities are based on one of two methods described by Bridgman [3]. Calculations based on Stokes' Law were used to determine the fall speed of the smallest particle size

group, whose entire bin range falls underneath the roughly 10 μm cut-off for which Bridgman asserts that Stokes' Law holds valid. The fall speeds for all other size bins were calculated using the algorithm developed by Norman Davies [10]. Both methods are discussed in detail in Chapter 2.

Following Miller, the source term is given as total gamma radiation activity rather than some other physical quantity such as total mass or total number of particles. Because activity fraction very closely follows mass fraction, the distribution and associated particle size bins remain appropriate and it can be justified to assume that particle size bins determined to contain exactly ten percent of the total mass of the stabilized cloud also contain about ten percent of the total activity of the cloud.

4. Results & Analysis

4.1 Results Overview

This chapter presents the results of predictions made by all three models studied along with comparisons to historic dose-rate contours taken from DNA-1251-EX. Each prediction is numerically scored against the observational data by determining the predictions values for measure of effectiveness (MOE) and normalized absolute difference (NAD). A presentation of results from the modified WRF code is given, followed by the results from HPAC and HYSPLIT. The last section presents the results from all three models studied against each other and discusses implications of those comparisons.

4.2 WRF Deposition Results

The modified WRF/Chem code was successfully implemented as a fallout model and compared to observational data taken from DNA-1251-EX. From the output of each simulation, dose-rates at various level contours were extracted and plotted against those same dose-rates highlighted from the observational data. From these plots a visual sense of how realistically the model simulates fallout can be inferred and a numerical score can be assigned.

The first simulation is from Operation Tumbler-Snapper: George, whose comparative contours with the modified WRF code are shown in Figure 7 through Figure 11. As with all of the simulations with any of the models, only basic accuracy can be gleaned from visual comparisons at high dose rates, while low-dose rate contour

predictions over a much greater area provide more useful information, both in terms of judging the qualitative and quantitative accuracy of the models as well as their implications as far as potential emergency planning and management. In the case of the George simulation, basic direction of the fallout for the highest dose-rates deviates just slightly from the observed data with some over-prediction at areas closer to ground zero. At lower dose-rate contours, namely those at $0.02\,{}^{R}\!/_{h}$ and $0.008\,{}^{R}\!/_{h}$, its easily seen that the slight misdirection at early simulation times results in slight over-prediction to the west and under-prediction to the east while preserving a fairly accurate description of the general area of fallout. It is interesting to note that at the lowest dose-rate contour, the lump feature seen just northwest of ground zero is emulated by the modified WRF simulation (Figure 11).

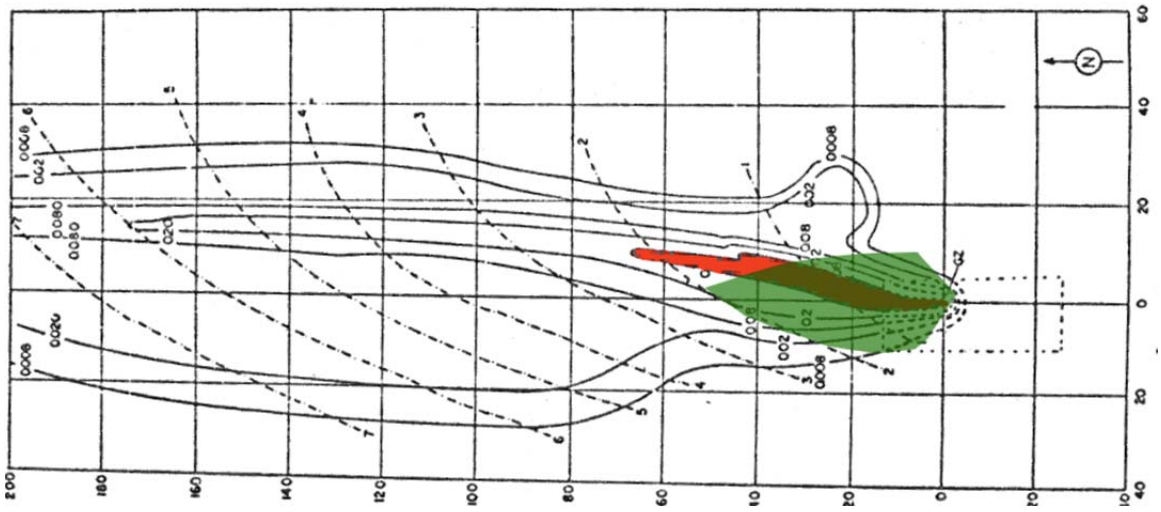

Figure 7. Fallout Pattern Predicted by Modified WRF Code (Green) as compared to Observationally-Based Data from Test Shot George at Dose-Rate Contour Level 0.8 R/h at H+1

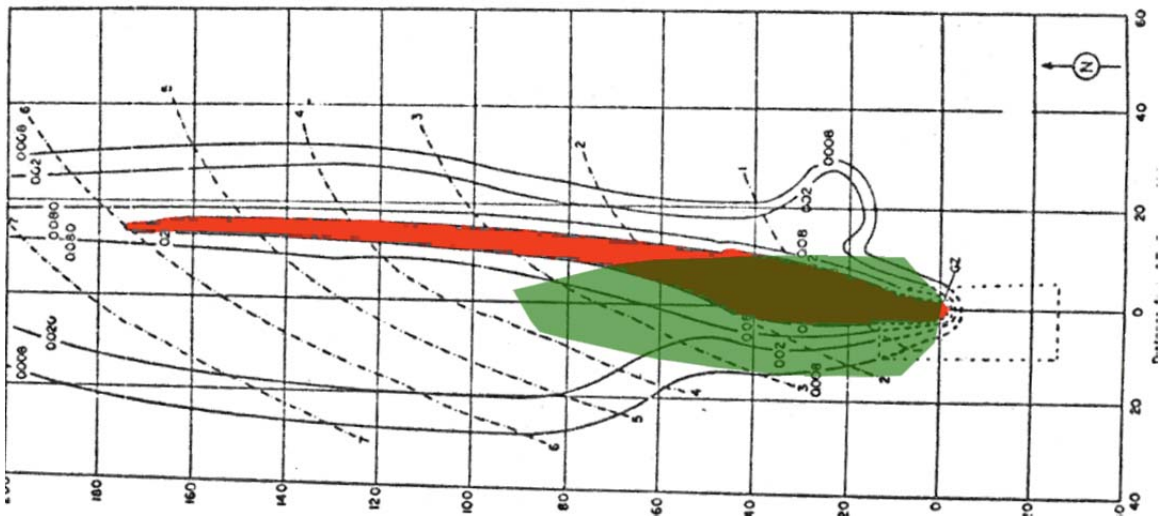

Figure 8. Fallout Pattern Predicted by Modified WRF Code (Green) as compared to Observationally-Based Data from Test Shot George at Dose-Rate Contour Level 0.2 R/h at H+1

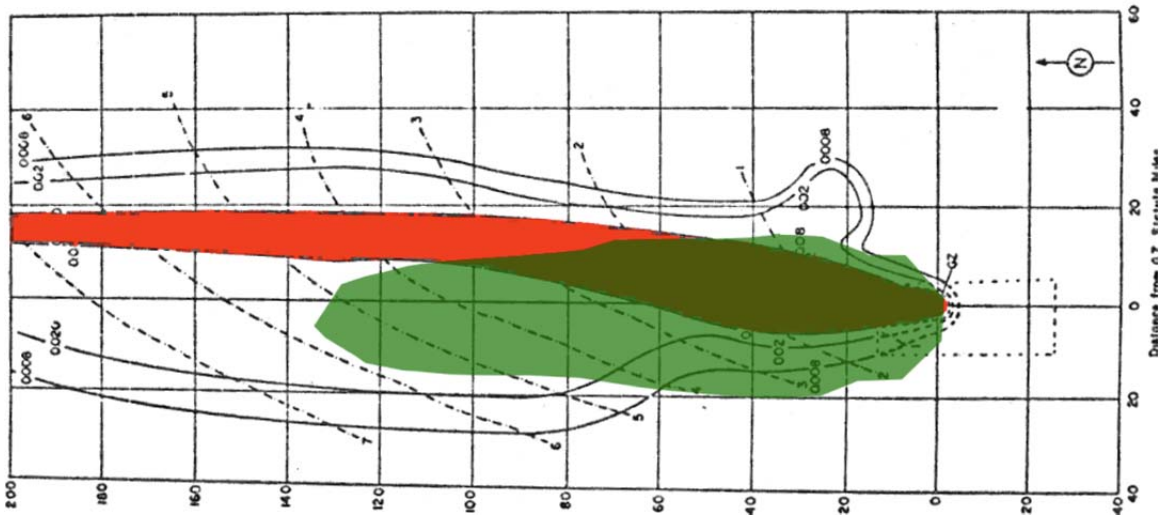

Figure 9. Fallout Pattern Predicted by Modified WRF Code (Green) as compared to Observationally-Based Data from Test Shot George at Dose-Rate Contour Level 0.08 R/h at H+1

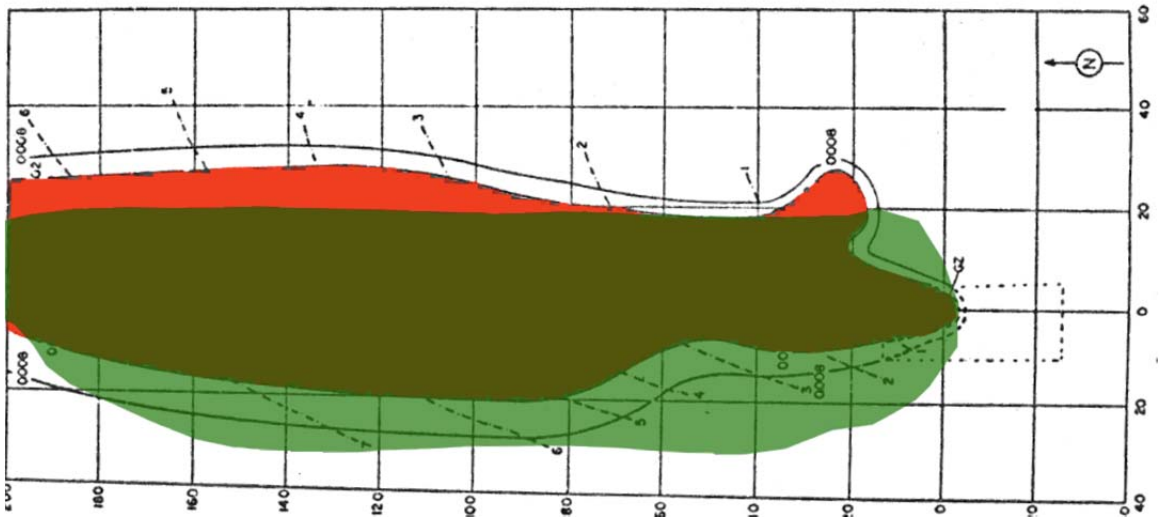

Figure 10. Fallout Pattern Predicted by Modified WRF Code (Green) as compared to Observationally-Based Data from Test Shot George at Dose-Rate Contour Level 0.02 R/h at H+1

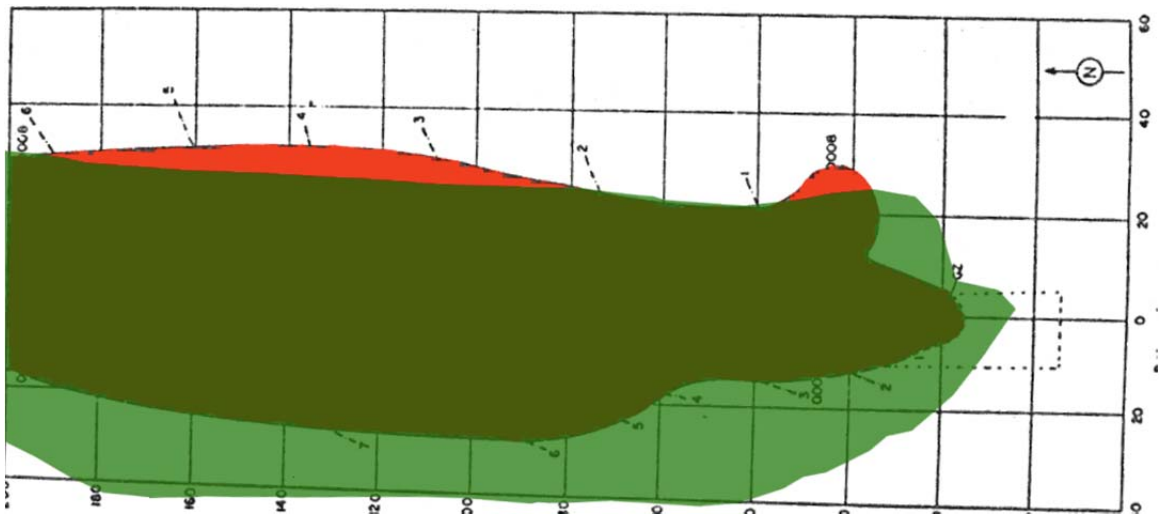

Figure 11. Fallout Pattern Predicted by Modified WRF Code (Green) as compared to Observationally-Based Data from Test Shot George at Dose-Rate Contour Level 0.08 R/h at H+1

The next test shot simulated was Operation Teapot: Zucchini, whose comparative contours are seen in Figure 12 through Figure 16. The basic direction of fallout at the highest dose-rates is even more accurately described by the modified WRF code than with the George simulation. As with that simulation some over-prediction at areas

closest to ground zero is noted along with under-prediction at areas farther away for contours 0.2 R/h and 0.08 R/h. The lowest two dose-rates (Figure 15 and Figure 16) highlight the ability of the WRF code to assimilate weather data and predict the direction of any particulate that exist in the atmosphere. While over-prediction is observed in the southeast direction, the simulation accurately predicts that at some point during deposition, fallout particulate is taken southeast and northeast.

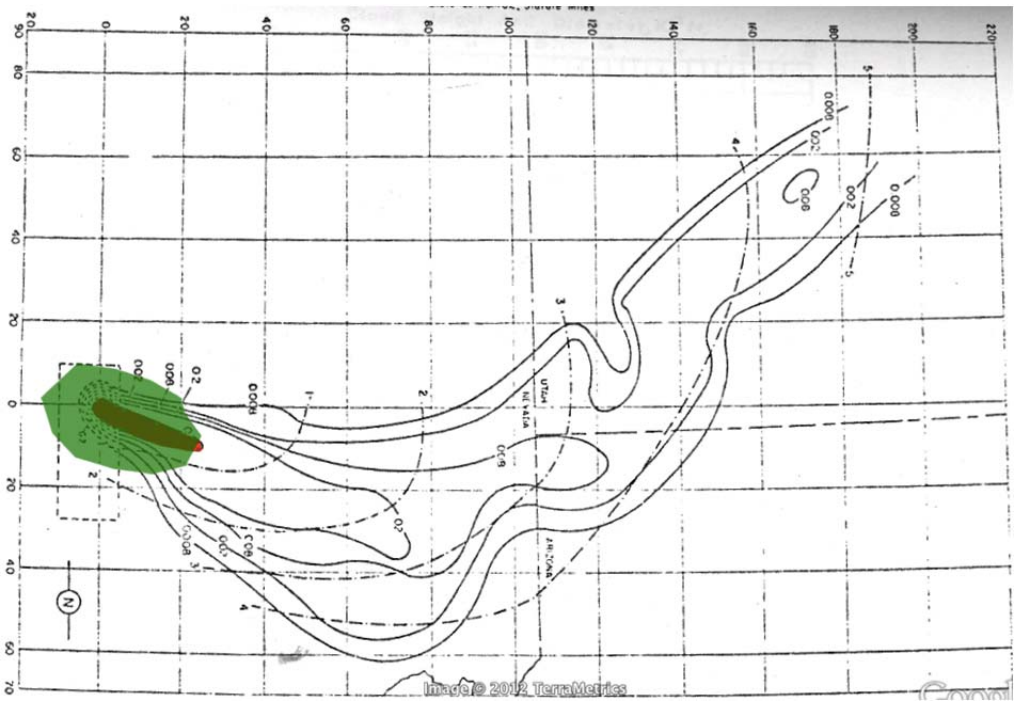

Figure 12. Fallout Pattern Predicted by Modified WRF Code (Green) as compared to Observationally-Based Data from Test Shot Zucchini at Dose-Rate Contour Level 0.8 R/h at H+1

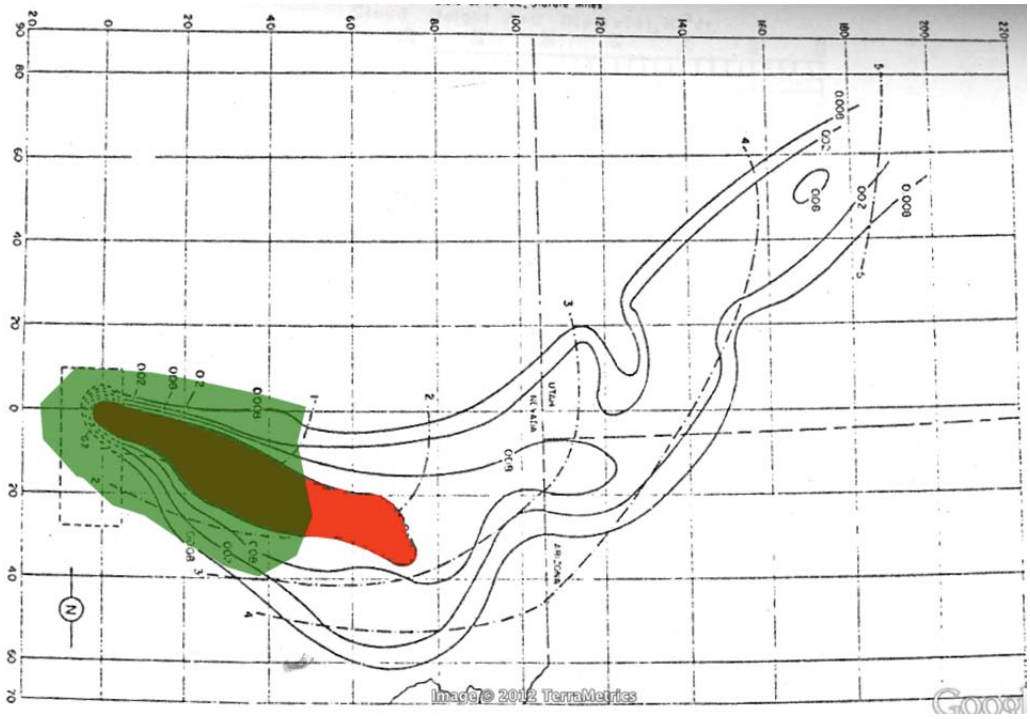

Figure 13. Fallout Pattern Predicted by Modified WRF Code (Green) as compared to Observationally-Based Data from Test Shot Zucchini at Dose-Rate Contour Level 0.2 R/h at H+1

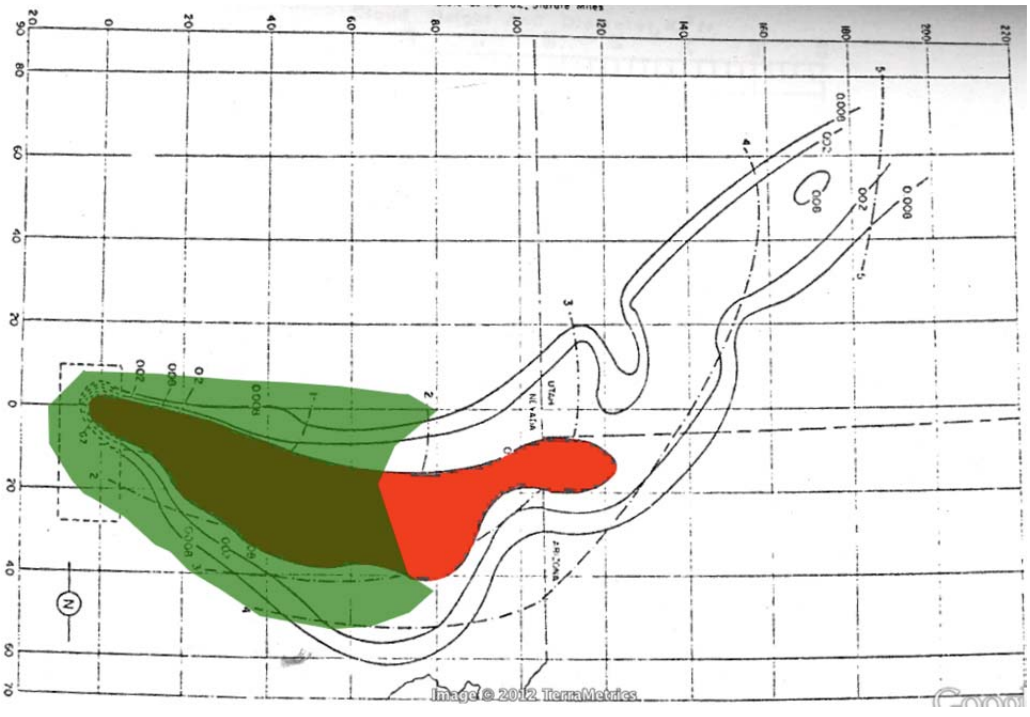

Figure 14. Fallout Pattern Predicted by Modified WRF Code (Green) as compared to Observationally-Based Data from Test Shot Zucchini at Dose-Rate Contour Level 0.08 R/h at H+1

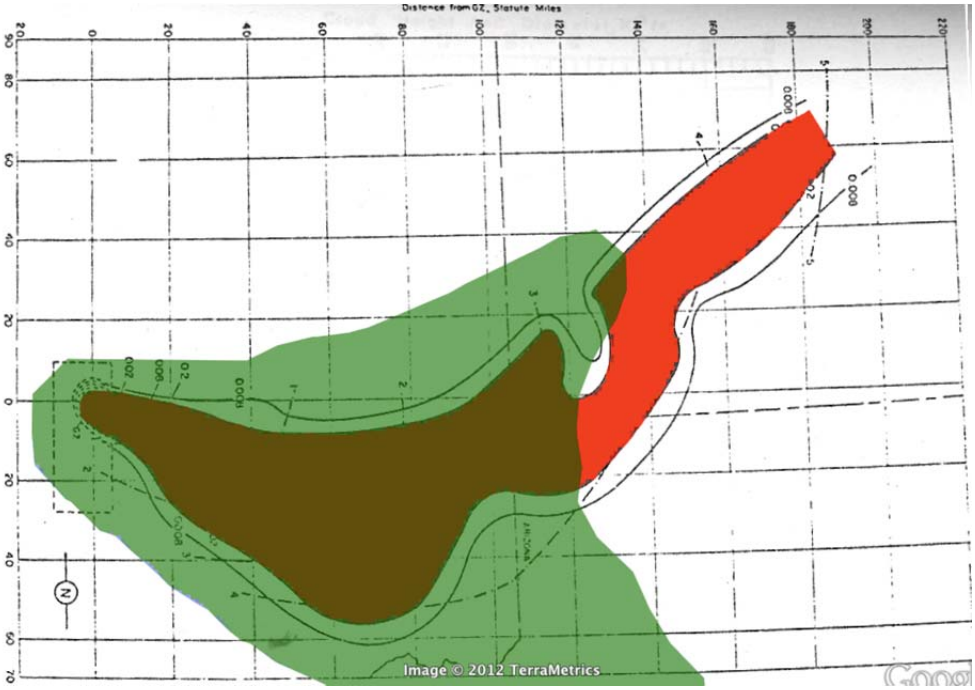

Figure 15. Fallout Pattern Predicted by Modified WRF Code (Green) as compared to Observationally-Based Data from Test Shot Zucchini at Dose-Rate Contour Level 0.02 R/h at H+1

Figure 16. Fallout Pattern Predicted by Modified WRF Code (Green) as compared to Observationally-Based Data from Test Shot Zucchini at Dose-Rate Contour Level 0.008 R/h at H+1

A third simulation is of Operation Pumbbob: Smoky, with comparisons being made at only two dose-rate contours due to the limited well-defined, well-separated contours in the data, as seen in Figure 17 Figure 18. Fairly severe under-prediction is observed for both contour levels, and the initial east-southeast direction of the fallout pattern is not well defined in the prediction which may be due to the fact that the code implemented is lacking an original, nuclear-detonation-specific cloud-rise module, which would include particulate at the lowest levels of the initial stabilized cloud as well as within the stem that would be picked up by low-altitude winds blowing in a different direction that those at higher altitudes. The modified WRF code does however predict the basic direction of the Smoky fallout with drastically greater accuracy than do the other two models compared, as will be seen in the next sections.

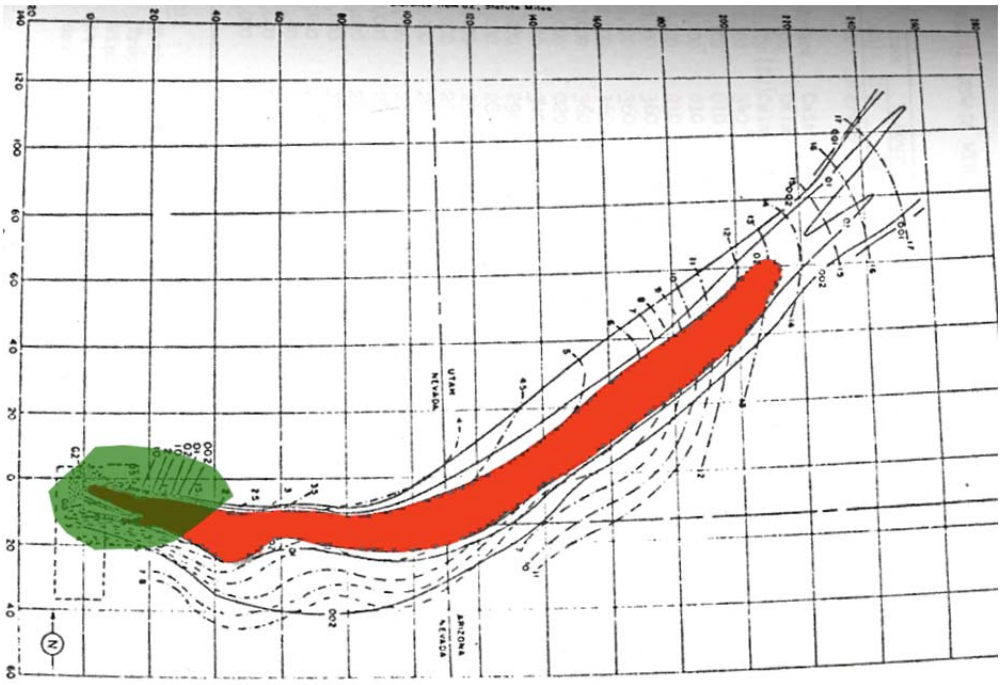

Figure 17. Fallout Pattern Predicted by Modified WRF Code (Green) as compared to Observationally-Based Data from Test Shot Smoky at Dose-Rate Contour Level 0.2 R/h at H+1

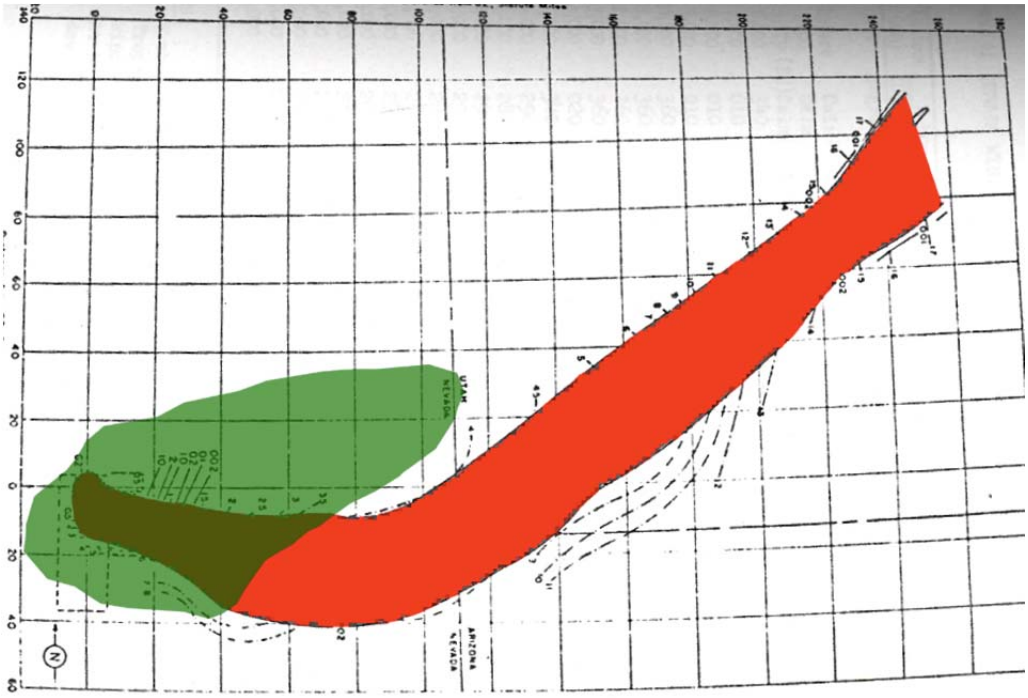

Figure 18. Fallout Pattern Predicted by Modified WRF Code (Green) as compared to Observationally-Based Data from Test Shot Smoky at Dose-Rate Contour Level 0.02 R/h at H+1

Table 2 presents the measure of effectiveness (MOE) and normalized absolute difference (NAD) scores for each of the simulations at each dose-rate level. For Zucchini and George simulations, basic accuracy of the prediction is reflected in the NAD scores, with the model performing most accurately at the lowest two dose-rates during the George simulation. The over-predicting tendencies during those same two simulations are reflected in the relatively low MOE y-coordinates. Those scores are presented graphically in two-dimensional MOE space in Figure 19.

Table 2. Summary of Quantitative Assessments of All Modified WRF Fallout Dose-Rate Predictions

WRF MOE/NAD Scores			
Test	Dose-Rate Contour	MOE	NAD
Zucchini	0.008 R/h	(0.970, 0.395)	0.439
	0.02 R/h	(0.721, 0.488)	0.418
	0.08 R/h	(0.634, 0.383)	0.522
	0.2 R/h	(0.707, 0.367)	0.517
	0.8 R/h	(1.00, 0.316)	0.520
George	0.008 R/h	(0.939, 0.690)	0.205
	0.02 R/h	(0.843, 0.716)	0.226
	0.08 R/h	(0.542, 0.374)	0.557
	0.2 R/h	(0.623, 0.394)	0.517
	0.8 R/h	(0.709, 0.285)	0.593
Smoky	0.02 R/h	(0.188, 0.259)	0.782
	0.2 R/h	(0.121, 0.258)	0.835

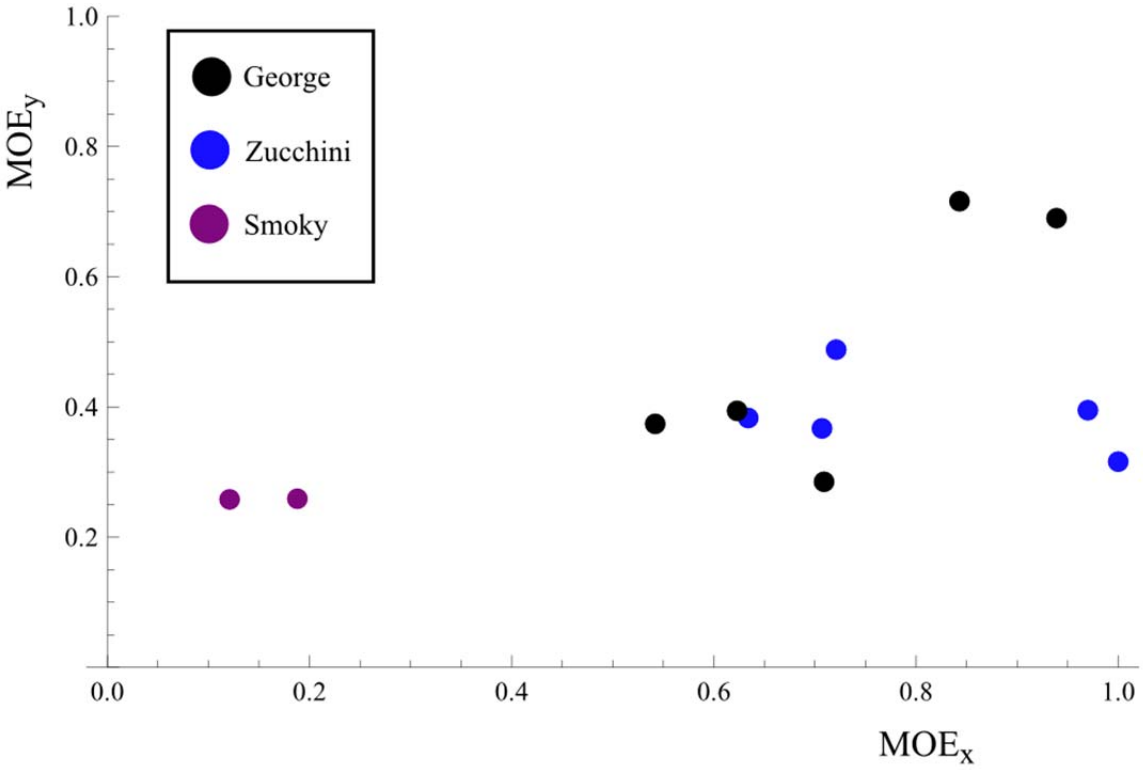

Figure 19. Measure of Effectiveness (MOE) Scores for All Modified WRF Fallout Simulations Plotted in Two-Dimensional MOE Space

4.3 HPAC Deposition Results

The same three test shots were successfully simulated using the Hazard Prediction & Assessment Capability (HPAC) model and the resulting dose-rate contours were plotted in the same manner against those from DNA-1251-EX. Quantitative assessment of the model's performance is presented following a discussion of how the simulations illustrate the model's typical behavior.

The first simulation, from the Tumbler-Snapper: George test shot, highlights what can be generally expected from an HPAC fallout prediction. These results are seen in Figure 20 through Figure 24. At the highest dose rote plotted, $0.8\,{}^{R}\!/_{h}$, it can be seen that the model correctly predicts the direction of deposition of the heavier particles that first fall to the ground. However, as lighter particles fall there is a clear northward shift in direction that HPAC fails to predict. Because HPAC predicts fallout to continue to occur in the initial more northeastward direction, more drastic false positives occur at lower dose-rate contours. The relatively simple shape of the patterns is typical of most HPAC predictions, and results in more detailed features, such as the lump feature seen in the $0.02\,{}^{R}\!/_{h}$ and $0.008\,{}^{R}\!/_{h}$ contours being missed.

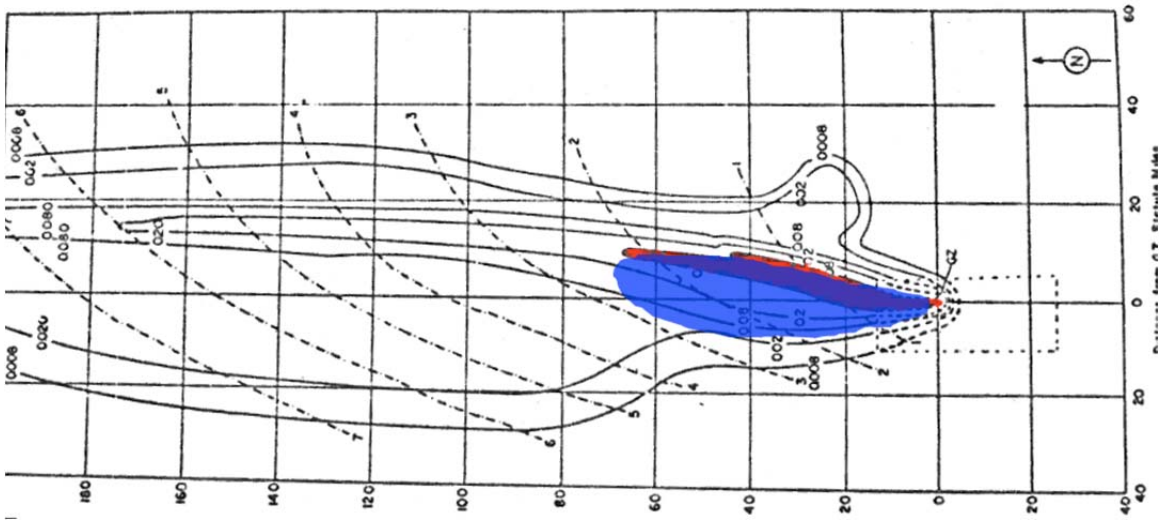

Figure 20. Fallout Pattern Predicted by HPAC (Blue) as compared to Observationally-Based Data from Test Shot George at Dose-Rate Contour Level 0.8 R/h at H+1

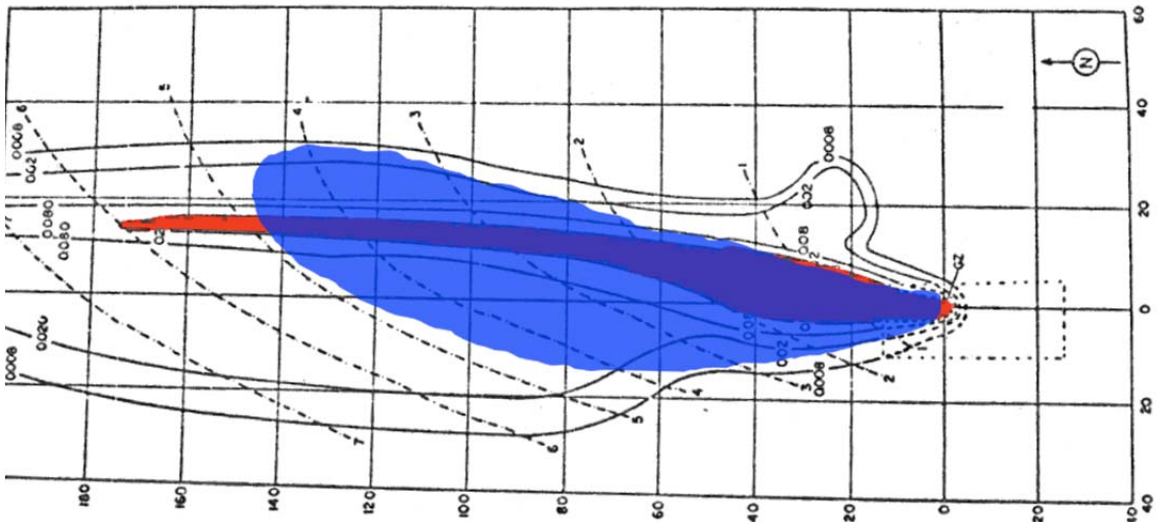

Figure 21. Fallout Pattern Predicted by HPAC (Blue) as compared to Observationally-Based Data from Test Shot George at Dose-Rate Contour Level 0.2 R/h at H+1

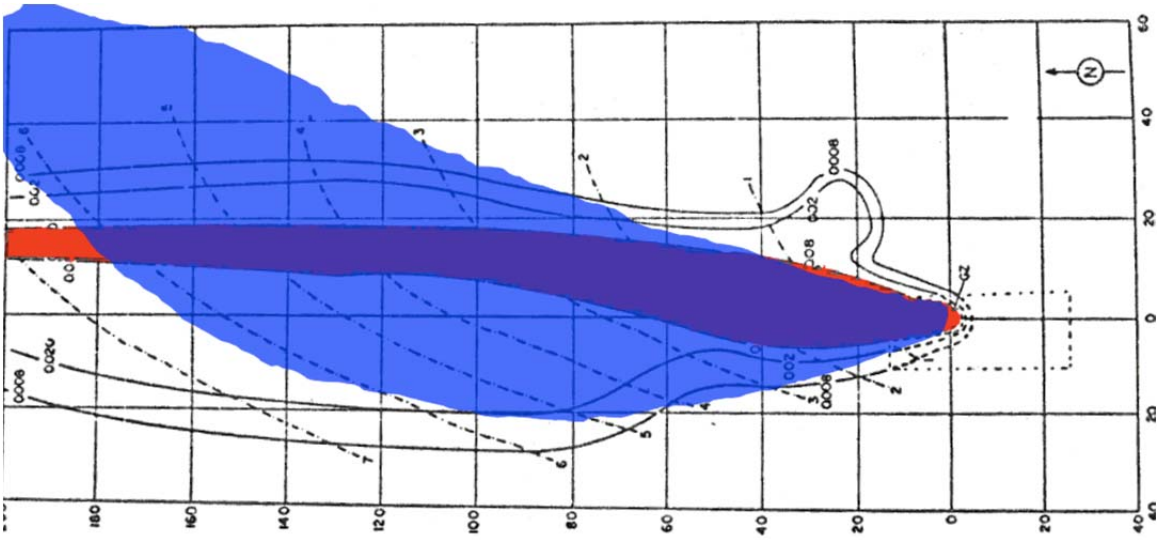

Figure 22. Fallout Pattern Predicted by HPAC (Blue) as compared to Observationally-Based Data from Test Shot George at Dose-Rate Contour Level 0.08 R/h at H+1

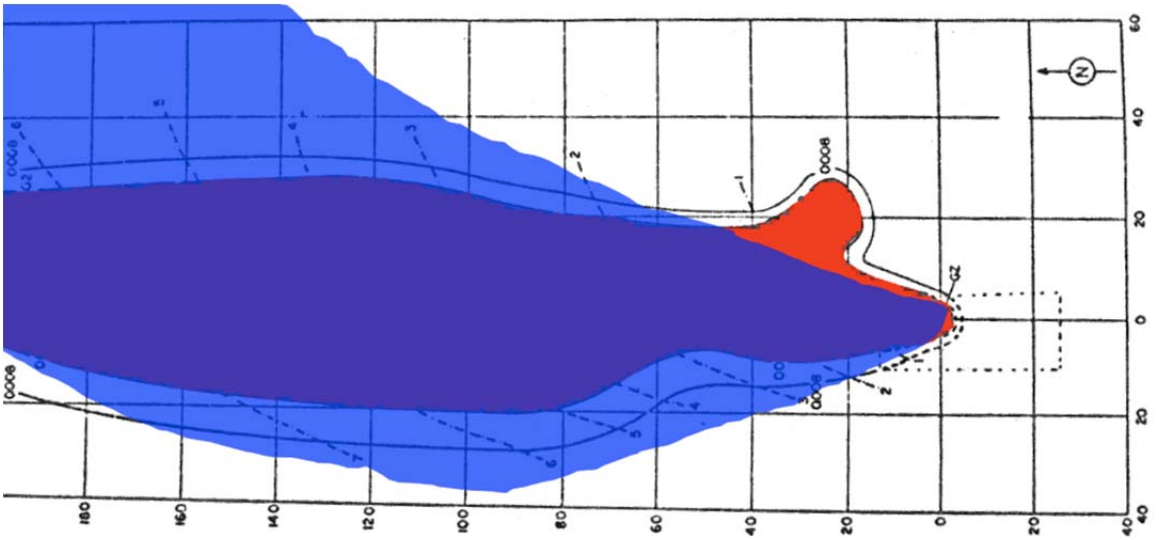

Figure 23. Fallout Pattern Predicted by HPAC (Blue) as compared to Observationally-Based Data from Test Shot George at Dose-Rate Contour Level 0.02 R/h at H+1

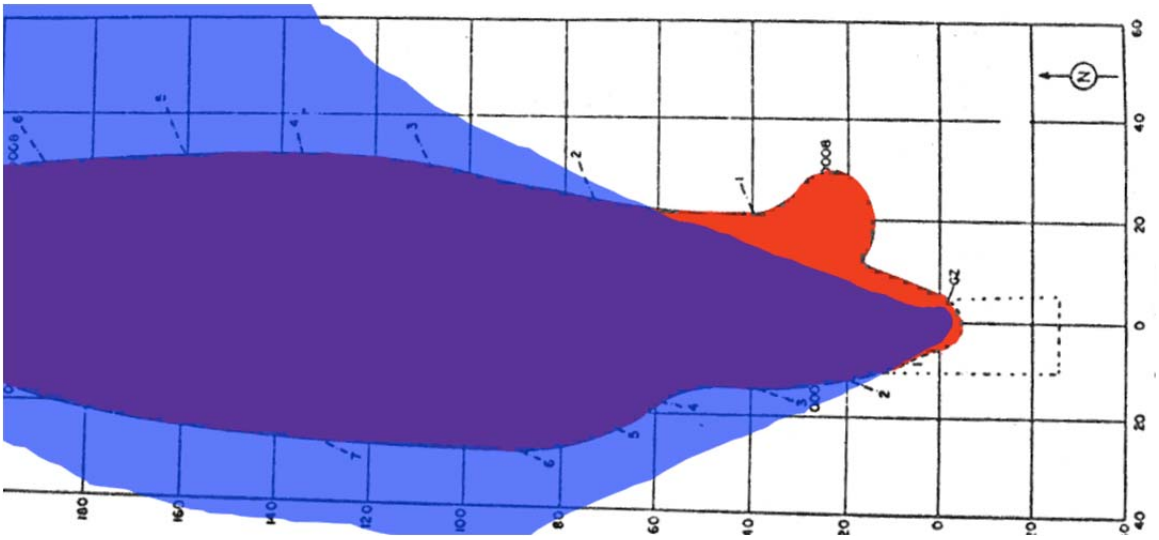

Figure 24. Fallout Pattern Predicted by HPAC (Blue) as compared to Observationally-Based Data from Test Shot George at Dose-Rate Contour Level 0.008 R/h at H+1

Similar qualitative features are seen in the predictions for the Zucchini test shot, shown in Figure 25 Figure 29. The initial direction of the early fallout seen in the 0.8 R/h contour is generally correct, but later changes in wind direction are not assimilated accurately into the prediction for particulate deposited later in time, resulting in increasing areas of over and under-prediction at lower dose-rate contours. A basic Gaussian-like pattern is again observed and unique features to the lower dose-rate contours of the observed Zucchini fallout pattern are not reflected in the HPAC prediction.

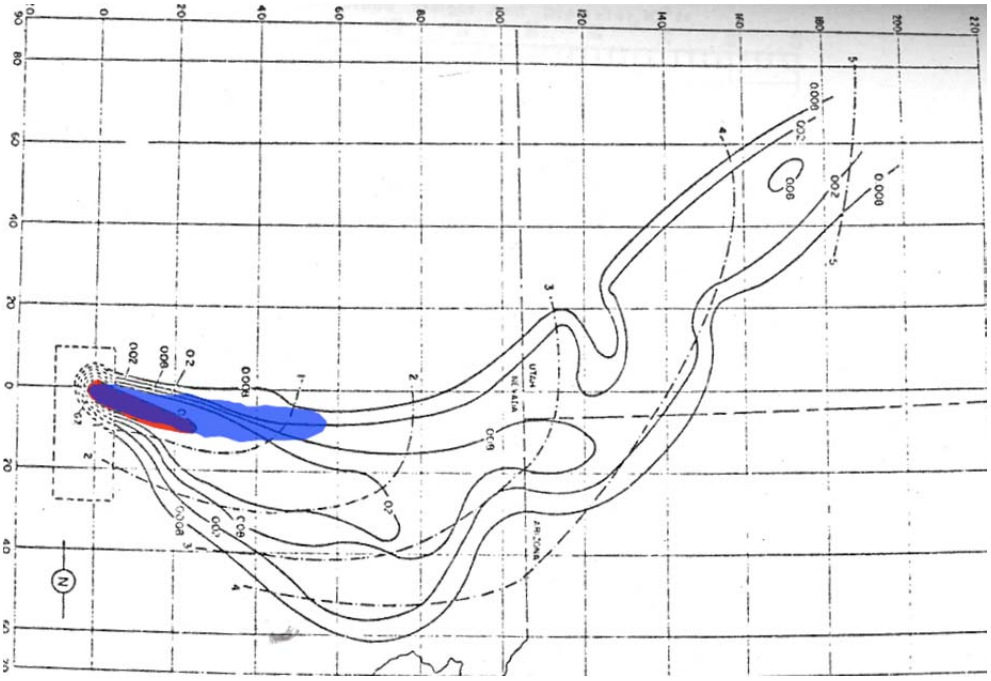

Figure 25. Fallout Pattern Predicted by HPAC (Blue) as compared to Observationally-Based Data from Test Shot Zucchini at Dose-Rate Contour Level 0.8 R/h at H+1

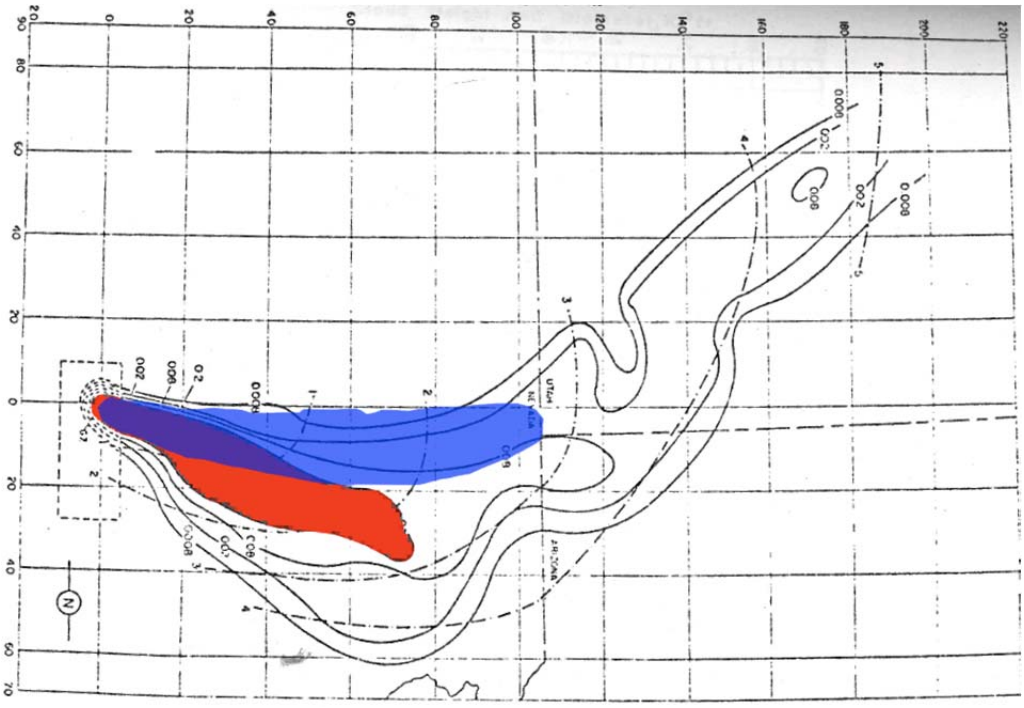

Figure 26. Fallout Pattern Predicted by HPAC (Blue) as compared to Observationally-Based Data from Test Shot Zucchini at Dose-Rate Contour Level 0.2 R/h at H+1

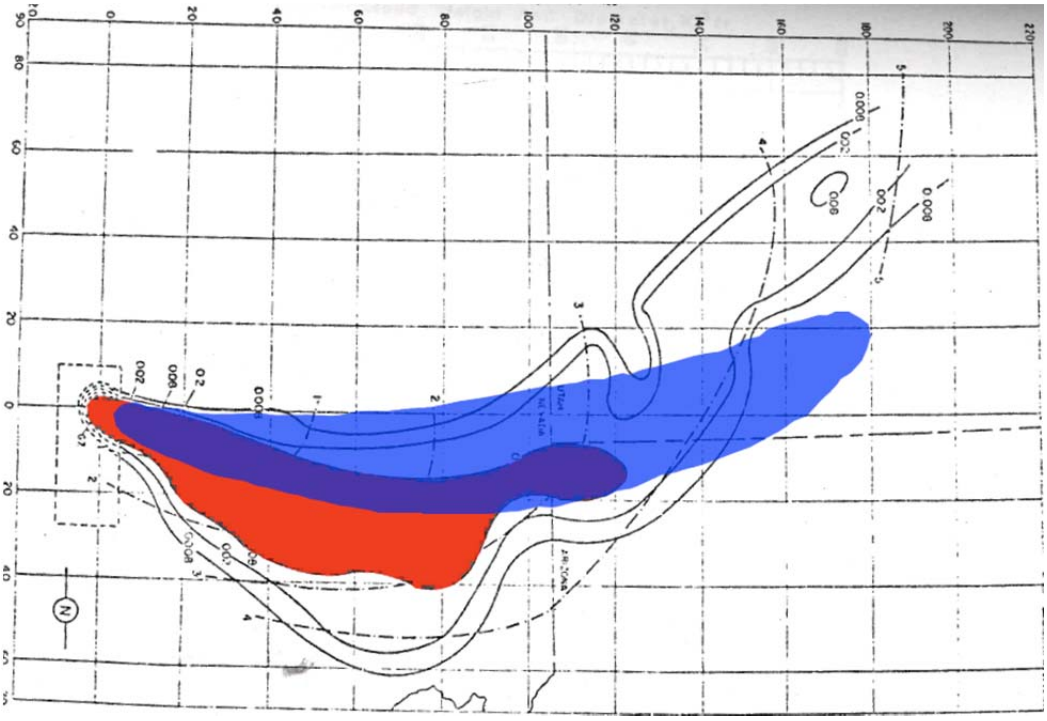

Figure 27. Fallout Pattern Predicted by HPAC (Blue) as compared to Observationally-Based Data from Test Shot Zucchini at Dose-Rate Contour Level 0.08 R/h at H+1

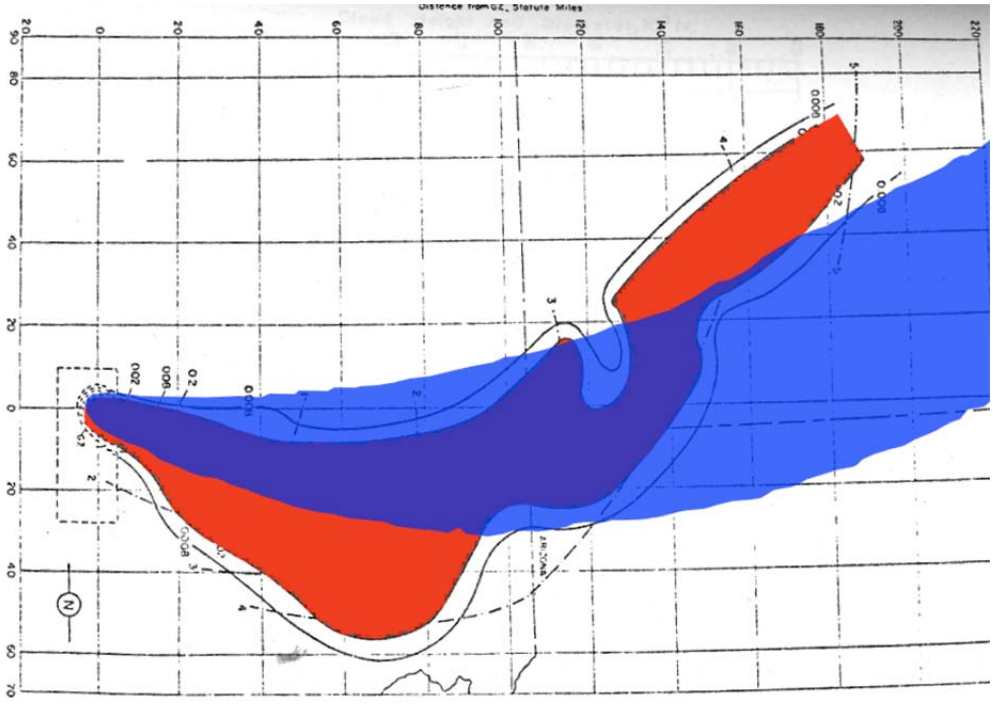

Figure 28. Fallout Pattern Predicted by HPAC (Blue) as compared to Observationally-Based Data from Test Shot Zucchini at Dose-Rate Contour Level 0.02 R/h at H+1

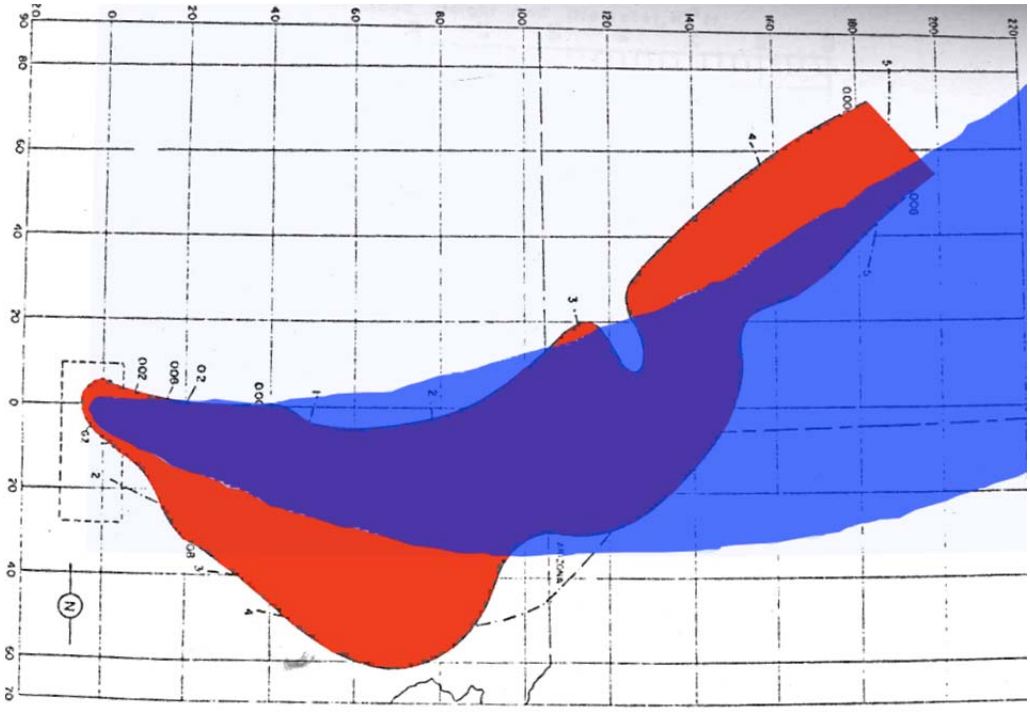

Figure 29. Fallout Pattern Predicted by HPAC (Blue) as compared to Observationally-Based Data from Test Shot Zucchini at Dose-Rate Contour Level 0.008 R/h at H+1

The HPAC results for the test shot from Operation Plumbbob: Smoky, seen in Figure 30 and Figure 31, again illustrate the general behavior of HPAC prediction and perhaps best highlights the potentially drastic consequences for operational fallout planning. The initial direction of the early fallout is not predicted accurately by the model, and because of HPAC's tendency to deposit fallout in the direction of the wind at stabilized cloud height with only slight curves in the pattern, the model completely fails to predict the area of observed fallout.

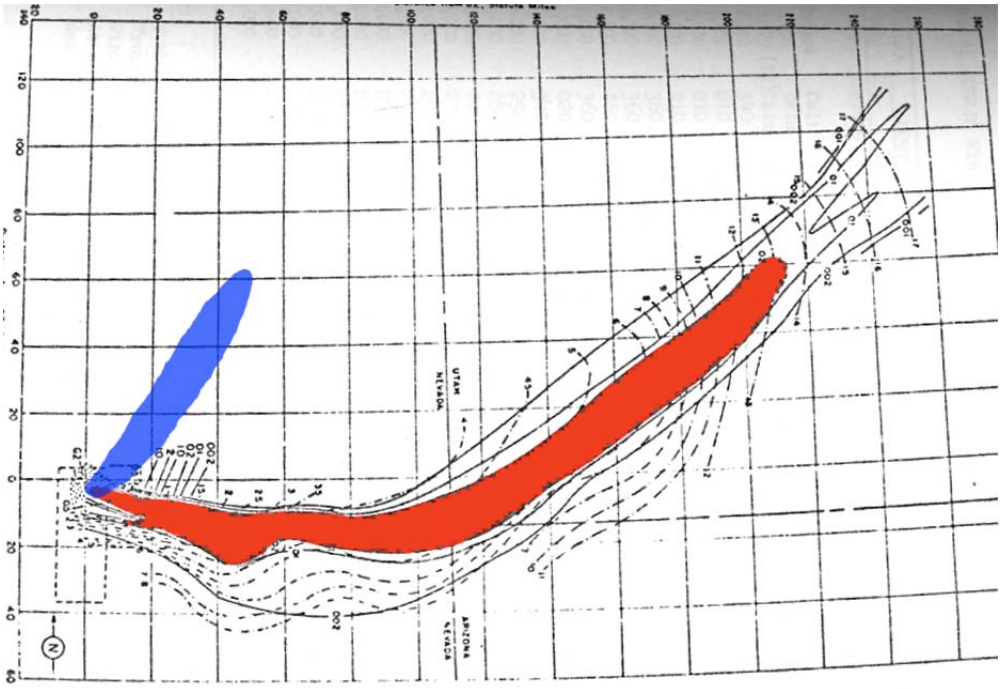

Figure 30. Fallout Pattern Predicted by HPAC (Blue) as compared to Observationally-Based Data from Test Shot Smoky at Dose-Rate Contour Level 0.2 R/h at H+1

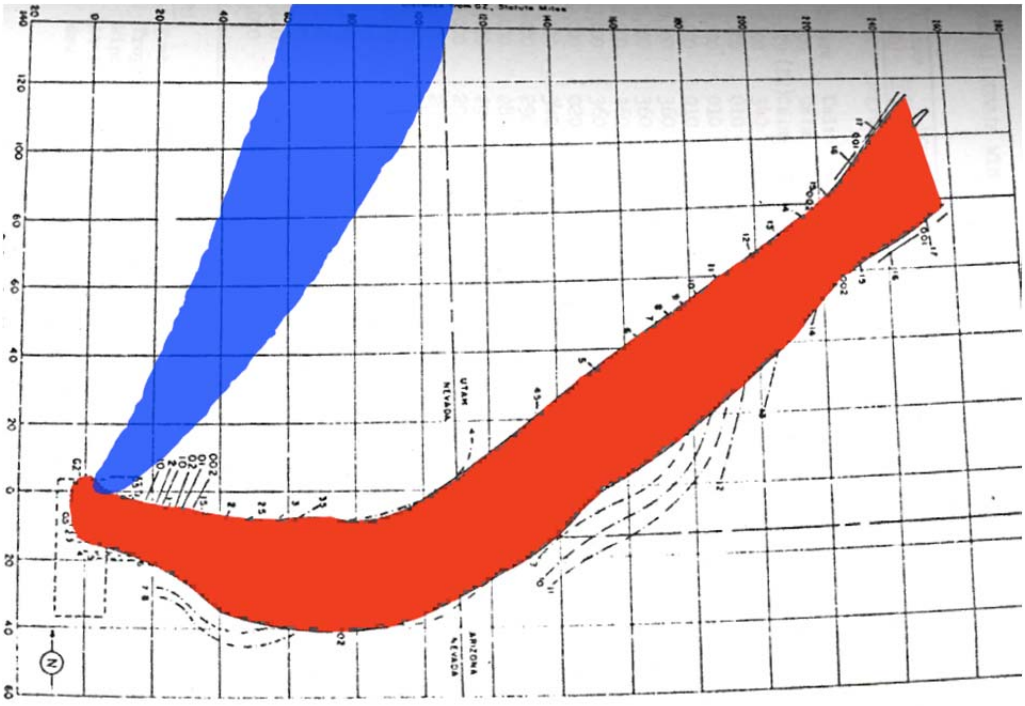

Figure 31. Fallout Pattern Predicted by HPAC (Blue) as compared to Observationally-Based Data from Test Shot Smoky at Dose-Rate Contour Level 0.02 R/h at H+1

The numerical scores of the HPAC simulations are presented in Table 3. Like the WRF model results, HPAC performed best in terms of normalized absolute difference (NAD) for the two highest dose-rate contours from the George simulation, though its score for those two runs are not quite as desirable as those for the WRF model. The extremely poor predictions for the Smoky simulation are reflected in measure of effectiveness (MOE) coordinates very close to zero and NAD scores very close to one. HPAC's tendency to over-predict is reflected in fairly low y-coordinates in its MOE scores. These MOE scores are shown for graphical comparison of the models performance between test simulations in Figure 32

.

Table 3. Summary of Quantitative Assessments of All HPAC Fallout Dose-Rate Predictions

HPAC MOE/NAD Scores			
Test	Dose-Rate Contour	MOE	NAD
Zucchini	0.008 R/h	(0.592, 0.463)	0.480
	0.02 R/h	(0.761, 0.358)	0.513
	0.08 R/h	(0.476, 0.304)	0.629
	0.2 R/h	(0.381, 0.268)	0.685
	0.8 R/h	(1.00, 0.245)	0.606
George	0.008 R/h	(0.915, 0.613)	0.266
	0.02 R/h	(1.00, 0.524)	0.312
	0.08 R/h	(0.948, 0.237)	0.621
	0.2 R/h	(0.867, 0.268)	0.591
	0.8 R/h	(0.957, 0.250)	0.604
Smoky	0.02 R/h	(0.005, 0.009)	0.994
	0.2 R/h	(0.016, 0.045)	0.976

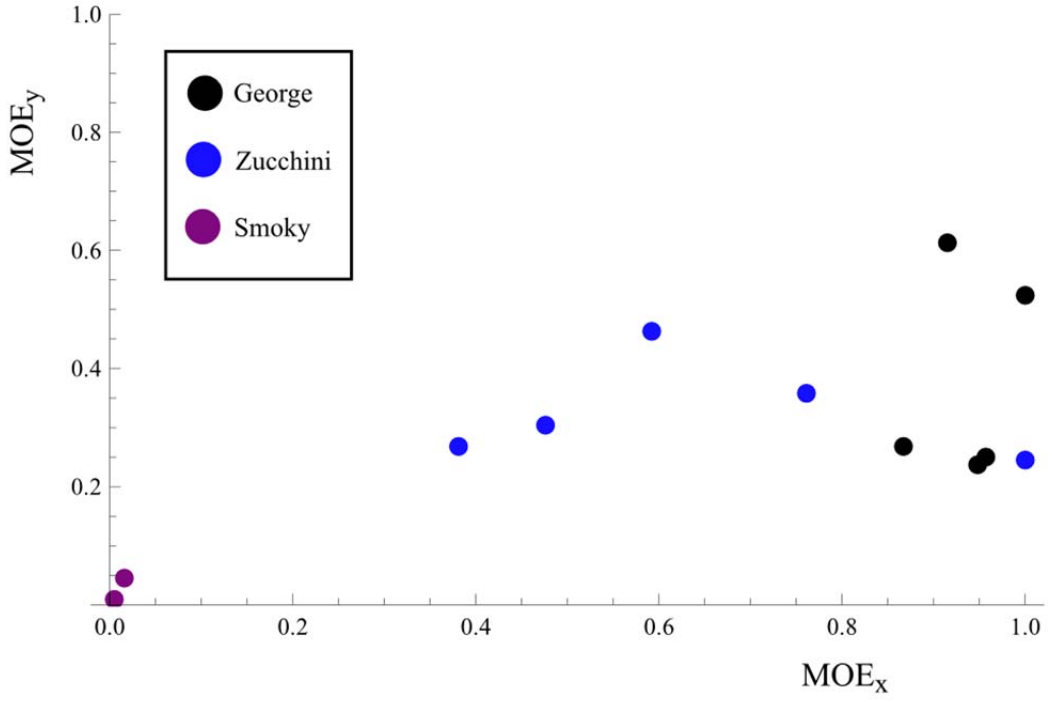

Figure 32. Measure of Effectiveness (MOE) Scores for All HPAC Fallout Simulations Plotted in Two-Dimensional MOE Space

4.4 HYSPLIT Deposition Results

The Hybrid Single Particle Lagrangian Integrated Trajectory (HYSPLIT) model was successfully employed to simulate fallout from test shots and the results were compared to dose-rate contours from DNA-1251-EX for analysis and numerical scoring. Because of how HYSPLIT uses single-particle Lagrangian methods for fallout prediction, deposition patterns are often broken up into multiple smaller contours, rather than single shape cleaner contours often seen with other models. Whereas the modified WRF code and especially the HPAC model tend to over-predict, HYSPLIT tends more towards under-prediction due to the scattering of smaller contours often observed. However, the complexity of the prediction methods in HYSPLIT result in more intricate patterns that often suggest a more accurate general direction of fallout deposition.

Contours from the George test-shot simulation are presented in Figure 33 through Figure 37. At the highest dose-rate HYSPLT fails to predict the initial north-northeast direction of the early fallout, however the general direction of the scattered contours suggest that model is somewhat reflecting the curvature of the early fallout. At lower-dose rates, the model predicts that later fallout will fall further west than was observed. This results in westward over-prediction and fairly severe under-prediction to the east.

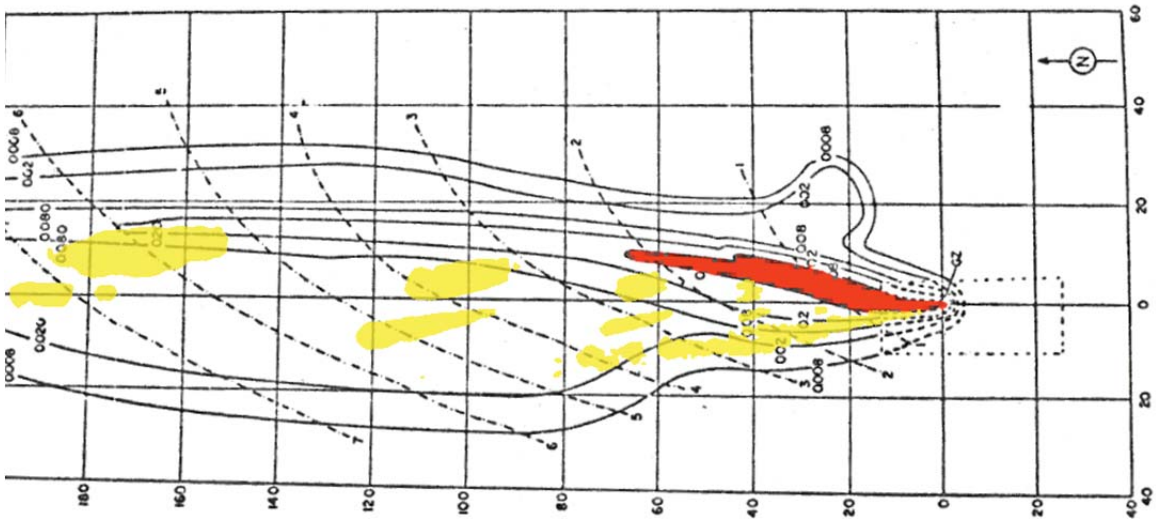

Figure 33. Fallout Pattern Predicted by HYSPLIT (Yellow) as compared to Observationally-Based Data from Test Shot George at Dose-Rate Contour Level 0.8 R/h at H+1

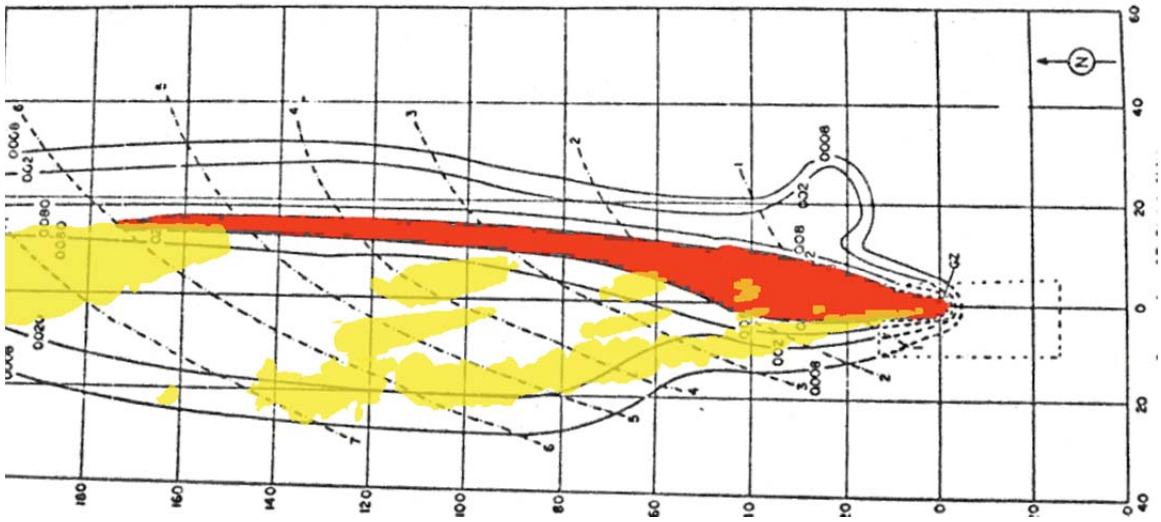

Figure 34. Fallout Pattern Predicted by HYSPLIT (Yellow) as compared to Observationally-Based Data from Test Shot George at Dose-Rate Contour Level 0.2 R/h at H+1

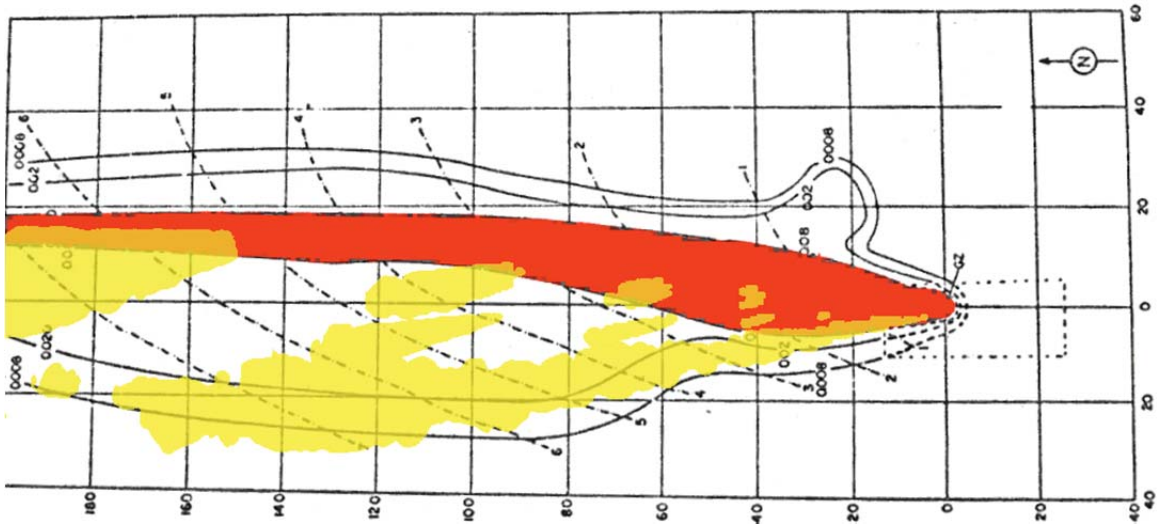

Figure 35. Fallout Pattern Predicted by HYSPLIT (Yellow) as compared to Observationally-Based Data from Test Shot George at Dose-Rate Contour Level 0.08 R/h at H+1

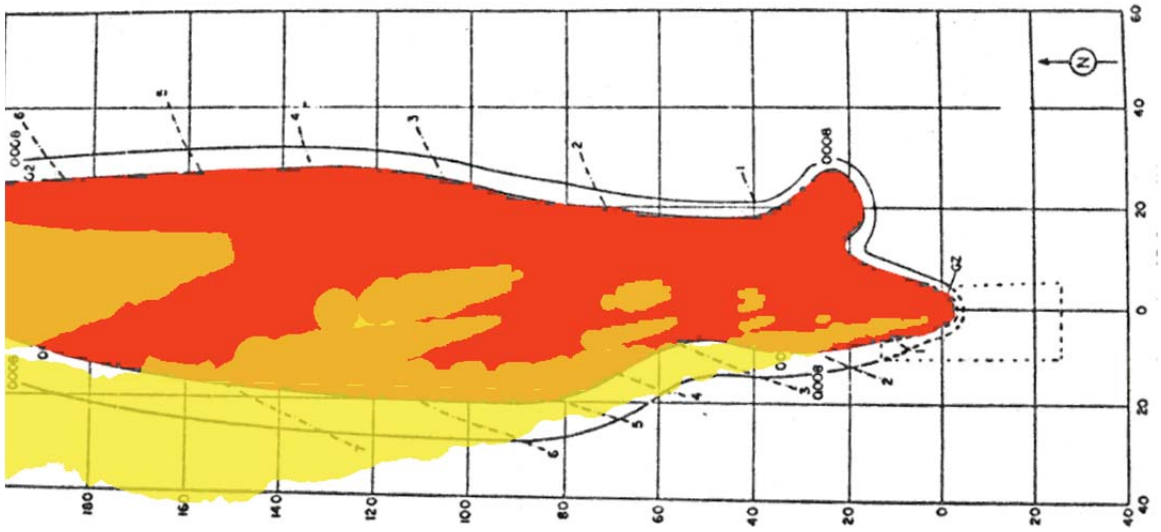

Figure 36. Fallout Pattern Predicted by HYSPLIT (Yellow) as compared to Observationally-Based Data from Test Shot George at Dose-Rate Contour Level 0.02 R/h at H+1

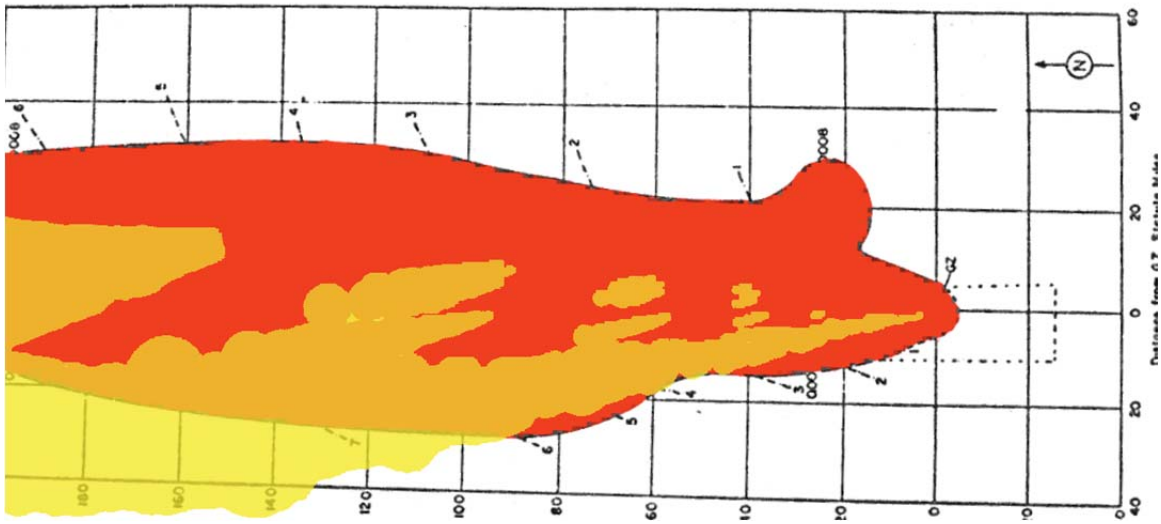

Figure 37. Fallout Pattern Predicted by HYSPLIT (Yellow) as compared to Observationally-Based Data from Test Shot George at Dose-Rate Contour Level 0.008 R/h at H+1

The predictions for operation Teapot: Zucchini, shown in Figure 38Figure 42, perhaps better illustrate HYSPLITs ability to account for more complex fallout patterns. At the lowest dose rate, the initial direction of early fallout is correctly predicted, and the area of over-prediction further from ground zero already begin to accurately reflect the

eventual shape of the fallout pattern for later deposited particles. At the lowest dose-rate, it is observed that some predicted deposition is northeast enough to overlap with that observed off-site, however there is a larger area of prediction that fails to curve northward as was observed.

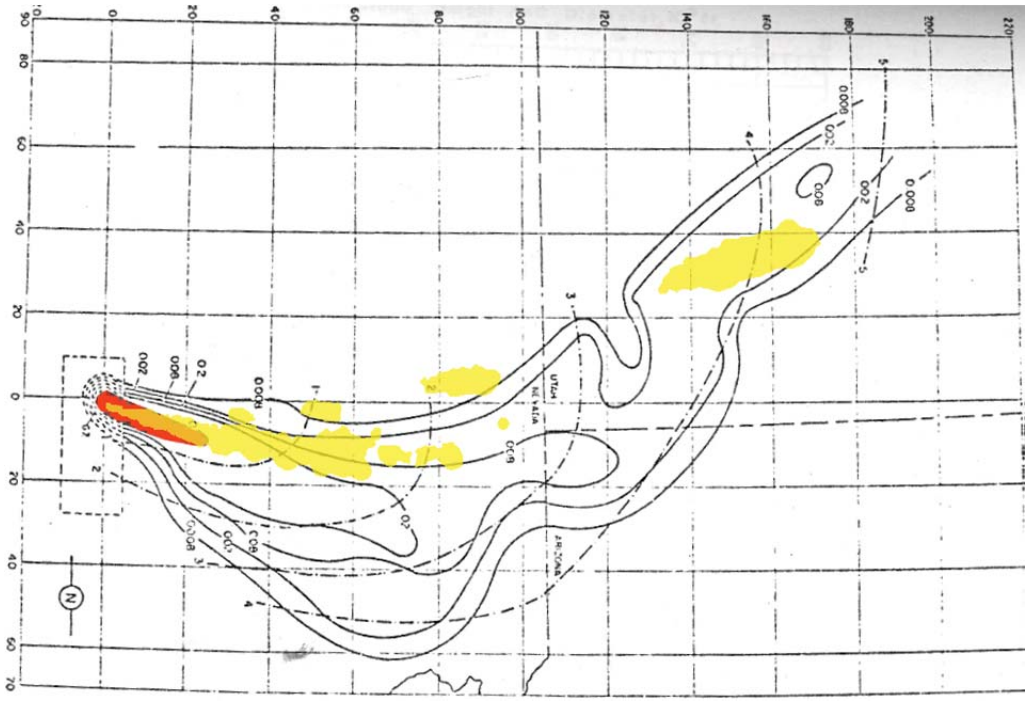

Figure 38. Fallout Pattern Predicted by HYSPLIT (Yellow) as compared to Observationally-Based Data from Test Shot Zucchini at Dose-Rate Contour Level 0.8 R/h at H+1

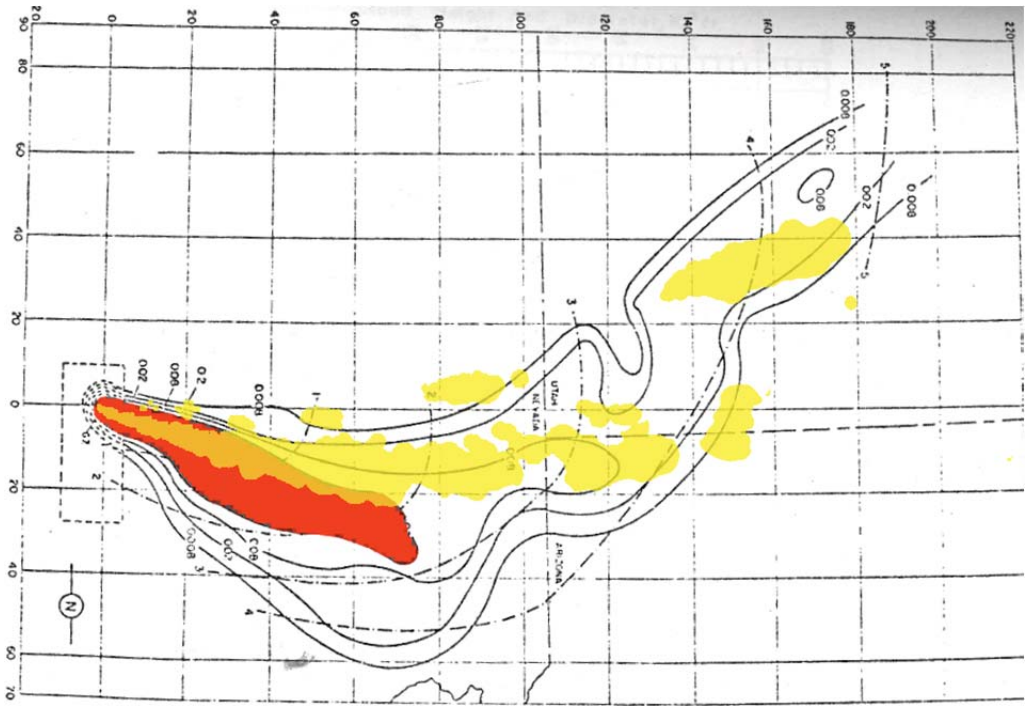

Figure 39. Fallout Pattern Predicted by HYSPLIT (Yellow) as compared to Observationally-Based Data from Test Shot Zucchini at Dose-Rate Contour Level 0.2 R/h at H+1

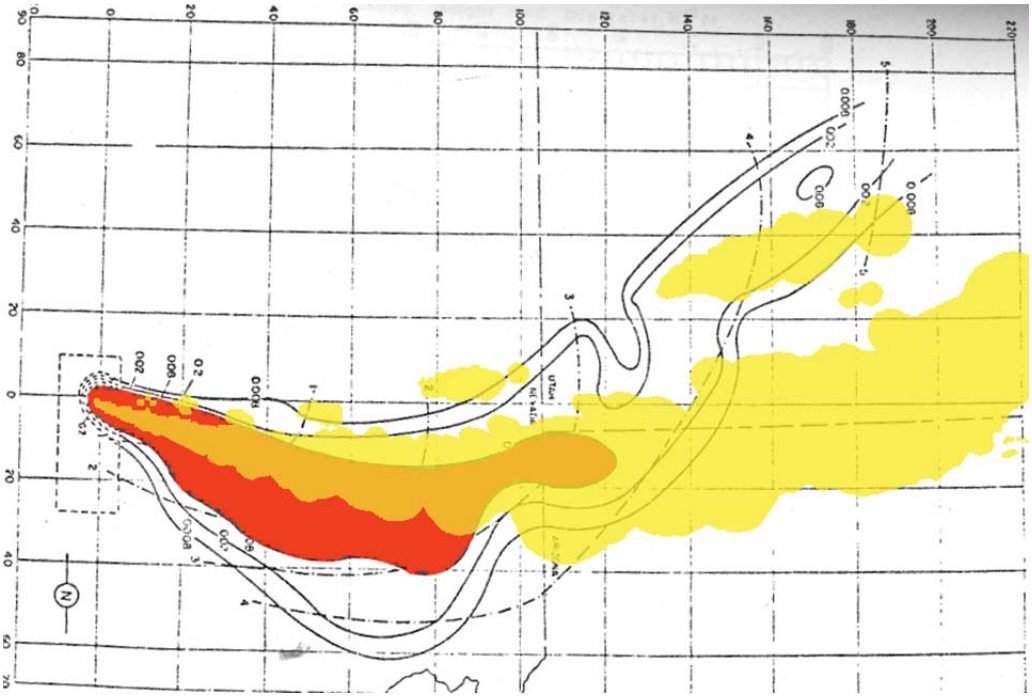

Figure 40. Fallout Pattern Predicted by HYSPLIT (Yellow) as compared to Observationally-Based Data from Test Shot Zucchini at Dose-Rate Contour Level 0.08 R/h at H+1

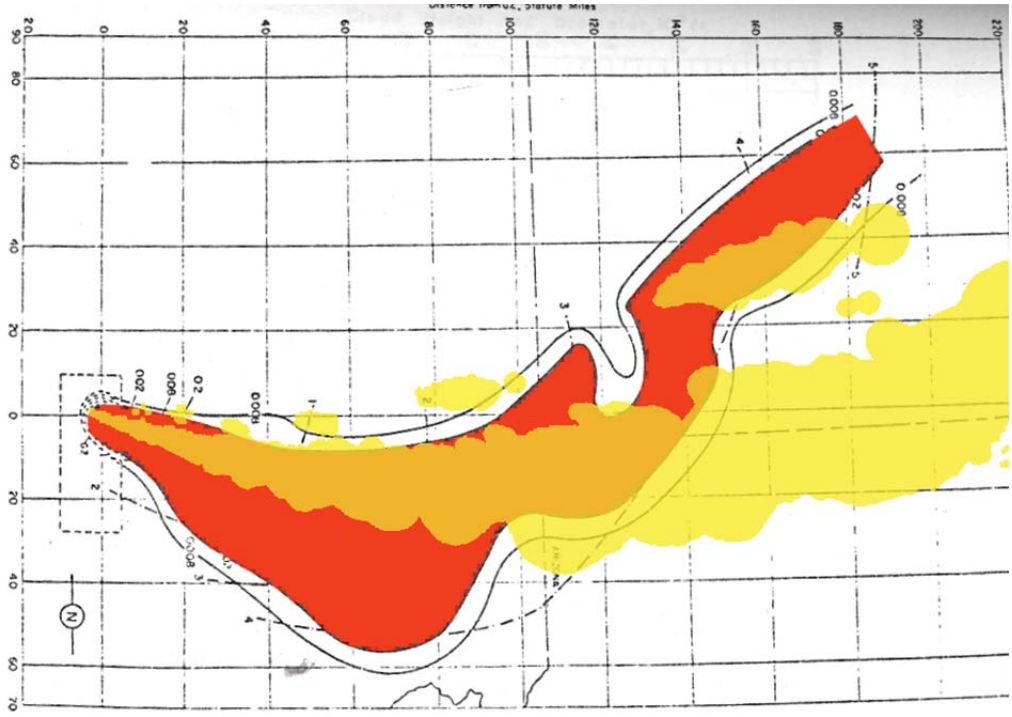

Figure 41. Fallout Pattern Predicted by HYSPLIT (Yellow) as compared to Observationally-Based Data from Test Shot Zucchini at Dose-Rate Contour Level 0.02 R/h at H+1

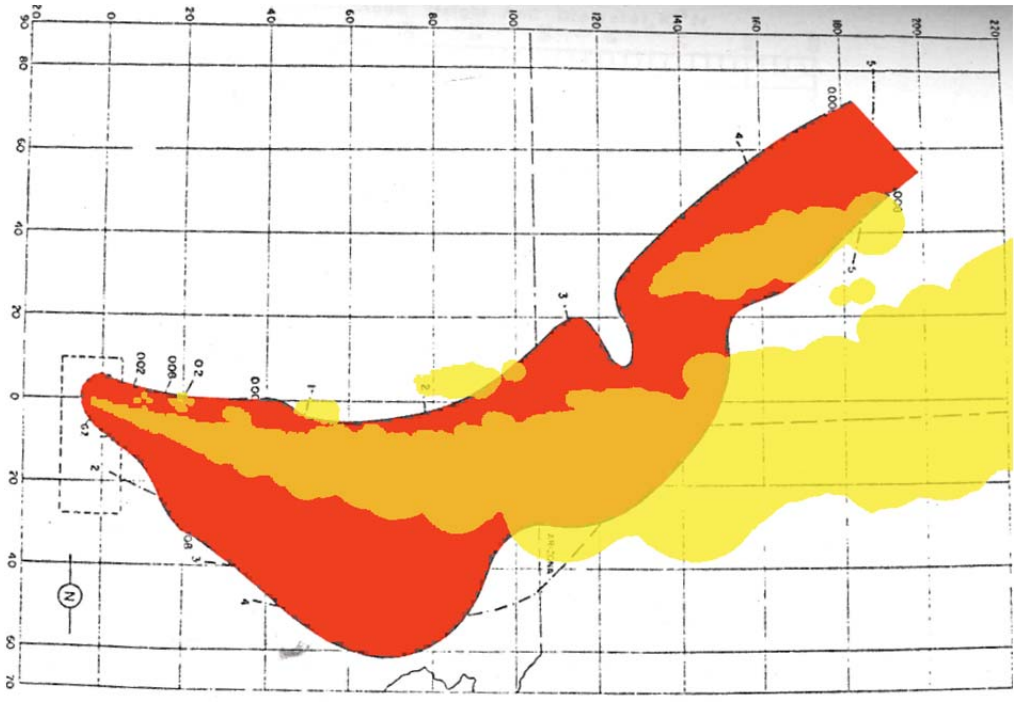

Figure 42. Fallout Pattern Predicted by HYSPLIT (Yellow) as compared to Observationally-Based Data from Test Shot Zucchini at Dose-Rate Contour Level 0.008 R/h at H+1

Like the HPAC simulation for the Smoky test-shot, HYSPLIT fails to predict the initial direction of the earliest fallout which results in severe degradation of its overall fallout prediction. This is illustrated in Figure 43 Figure 44. However unlike HPAC, the general direction of the scattered contours does eventually reflect the eastward direction of some fallout followed by a fairly sharp northward turn, mitigating at least somewhat the potential operational consequences for fallout prediction.

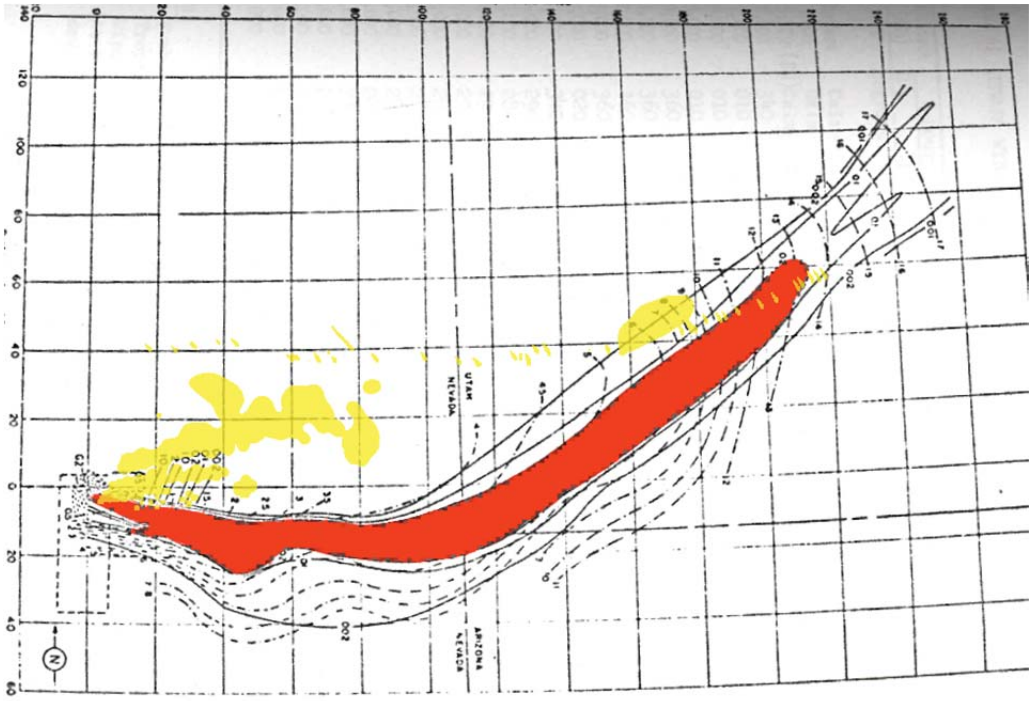

Figure 43. Fallout Pattern Predicted by HYSPLIT (Yellow) as compared to Observationally-Based Data from Test Shot Smoky at Dose-Rate Contour Level 0.2 R/h at H+1

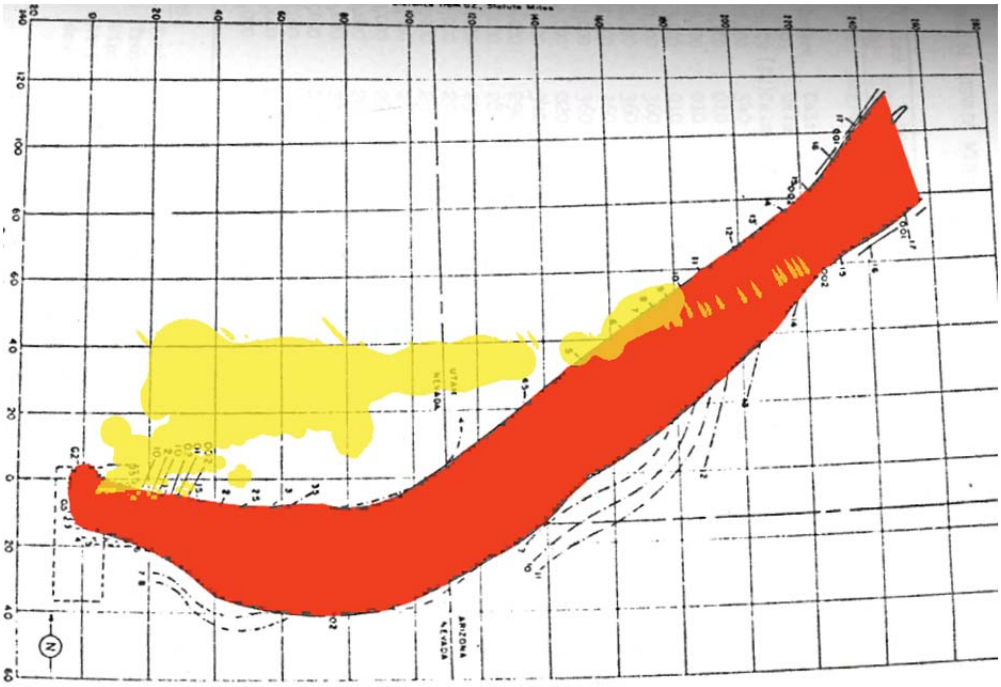

Figure 44. Fallout Pattern Predicted by HYSPLIT (Yellow) as compared to Observationally-Based Data from Test Shot Zucchini at Dose-Rate Contour Level 0.8 R/h at H+1

Table 4 summarizes the numerical assessments of the HYSPLIT simulations at all dose-rate levels compared. Because of the model's tendency to scatter contours widely over an area, fairly severe under-prediction is reflected in the x-coordinate of many of the MOE scores and the fact that there are no NAD scores that could be considered as desirable as some of the top scores from the modified WRF and HPAC simulations. However, these scores may be misleading in terms of judging potential operational value, as it is likely that general direction of predicted contours rather than absolute areas would inform emergency planning decisions. A graphical comparison of MOE scores between the HYSPLIT simulations is shown in Figure 45.

Table 4. Summary of Quantitative Assessments of All HYSPLIT Fallout Dose-Rate Predictions

HYSPLIT MOE/NAD Scores			
Test	Dose-Rate Contour	MOE	NAD
Zucchini	0.008 R/h	(0.431, 0.465)	0.553
	0.02 R/h	(0.457, 0.380)	0.585
	0.08 R/h	(0.612, 0.368)	0.540
	0.2 R/h	(0.545, 0.272)	0.637
	0.8 R/h	(1.00, 0.379)	0.450
George	0.008 R/h	(0.365, 0.663)	0.529
	0.02 R/h	(0.322, 0.467)	0.619
	0.08 R/h	(0.111, 0.266)	0.843
	0.2 R/h	(0.234, 0.133)	0.830
	0.8 R/h	(0.263, 0.114)	0.840
Smoky	0.02 R/h	(0.067, 0.133)	0.911
	0.2 R/h	(0.042, 0.021)	0.972

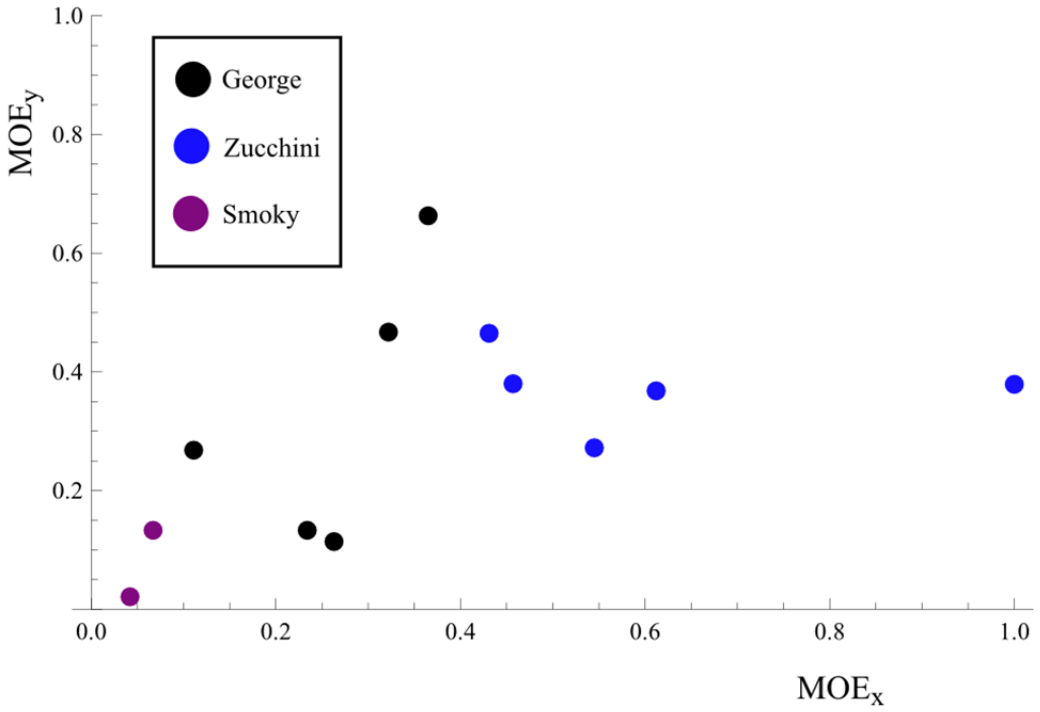

Figure 45. Measure of Effectiveness (MOE) Scores for All HYSPLIT Fallout Simulations Plotted in Two-Dimensional MOE Space

4.5 Comparative Analysis

It is asserted that even with its limitations, such as not having an explicit nuclear-detonation cloud rise module, the modified WRF code predicts fallout at least slightly more accurately, according to observational data, than does HPAC or HYSPLIT. This is due to the fact that WRF is at its core a highly-complex inline operational weather model that is able to better assimilate and interpolate meteorological variables from historic weather data, and use these variables to determine the direction of injected particulate. Visual inspection of the results from the simulations from all three models suggest that qualitatively, the modified WRF model has the potential to evolve into a more desirable operational tool than the currently employed models.

Table 5. Comparison of Measure-of-Effectiveness (MOE) and Normalized Absolute Difference (NAD) Scores between All Three Models Studied

MOE/NAD Scores For All Three Models							
		WRF		HPAC		HYSPLIT	
Test	Dose-Rate Contour	MOE	NAD	MOE	NAD	MOE	NAD
Zucchini	0.008 R/h	(0.970, 0.395)	0.439	(0.592, 0.463)	0.480	(0.431, 0.465)	0.553
	0.02 R/h	(0.721, 0.488)	0.418	(0.761, 0.358)	0.513	(0.457, 0.380)	0.585
	0.08 R/h	(0.634, 0.383)	0.522	(0.476, 0.304)	0.629	(0.612, 0.368)	0.540
	0.2 R/h	(0.707, 0.367)	0.517	(0.381, 0.268)	0.685	(0.545, 0.272)	0.637
	0.8 R/h	(1.00, 0.316)	0.520	(1.00, 0.245)	0.606	(1.00, 0.379)	0.450
George	0.008 R/h	(0.939, 0.690)	0.205	(0.915, 0.613)	0.266	(0.365, 0.663)	0.529
	0.02 R/h	(0.843, 0.716)	0.226	(1.00, 0.524)	0.312	(0.322, 0.467)	0.619
	0.08 R/h	(0.542, 0.374)	0.557	(0.948, 0.237)	0.621	(0.111, 0.266)	0.843
	0.2 R/h	(0.623, 0.394)	0.517	(0.867, 0.268)	0.591	(0.234, 0.133)	0.830
	0.8 R/h	(0.709, 0.285)	0.593	(0.957, 0.250)	0.604	(0.263, 0.114)	0.840
Smoky	0.02 R/h	(0.188, 0.259)	0.782	(0.005, 0.009)	0.994	(0.067, 0.133)	0.911
	0.2 R/h	(0.121, 0.258)	0.835	(0.016, 0.045)	0.976	(0.042, 0.021)	0.972

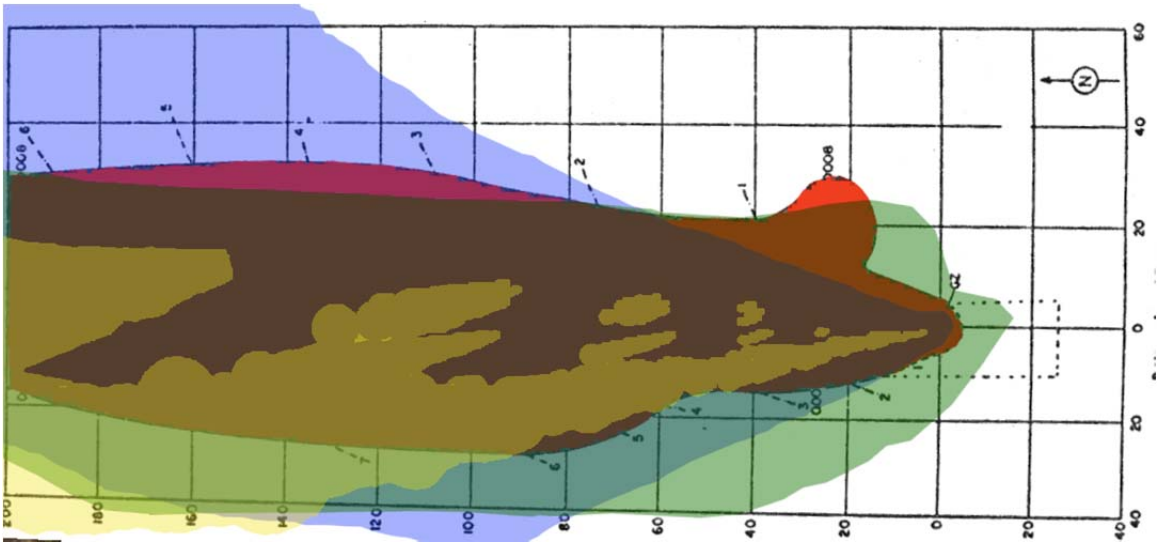

Figure 46. George Test-Shot 0.008 R/h Dose-Rate Contours: WRF (Green), HPAC (Blue), HYSPLIT (Yellow), and DNA-1251-EX Observational Data (Red)

For simulation of the George test detonation, all three models successfully overlapped with the general northward direction of the fallout, as seen in Figure 46. Because of the relatively simple pattern of dose-rate contours observed after this test-shot, HPAC simulations can be expected to encompass the vast majority of the area where fallout at low-levels was observed with over-prediction expected in both eastward and westward directions. This expectation is generally reflected in the model, though HPAC incorrectly suggests that fallout patterns will start to curve eastward. HYSPLIT on the other-hand suggests a slightly westward tilt to the general direction of fallout. The modified WRF code also somewhat under-predicts along the eastern side of the predicted fallout, but generally maintains an accurate northward direction of fallout. The modified WRF code is the only model that even somewhat reflected the lump feature observed just to the northeast of ground zero for the lowest dose-rate contours.

Figure 47 comparatively displays the MOE scores for the George simulations for all three models. In two dimensional MOE space, HPAC simulations can generally be expected to have lower y-coordinates because of its tendency to over-predict, while HYSPLIT scores can often be expected to have lower x-coordinates because of its tendency to under predict. This expectation is at least somewhat observed in the plot of Figure 47.

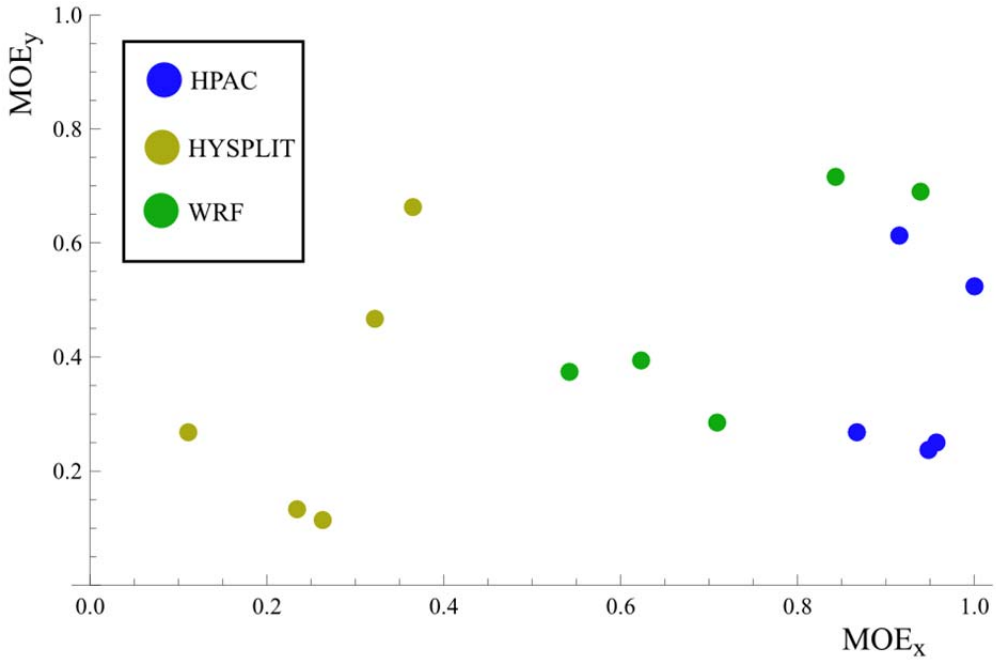

Figure 47. Measure of Effectiveness (MOE) Scores from All Three Models for Test Shot George

For the Zucchini test-shot simulation all three models successfully predicted a general eastward trend to deposited fallout over time (see Figure 48). Because of the more complicated shape of the fallout pattern, differences in how each model is able to predict become better exposed. While the HPAC and HYSPLIT models both have some overlap with the northeast corner of the observed fallout contour at the lowest dose-rate-levels, only the modified WRF code is able to predict a northward bend in the fallout

sharp enough to significantly reflect the observed pattern. The modified WRF model is also the only one that is able to account for both southeast and northeast directions of deposited fallout at different points in time, even though the model does over-predict in the southeast direction.

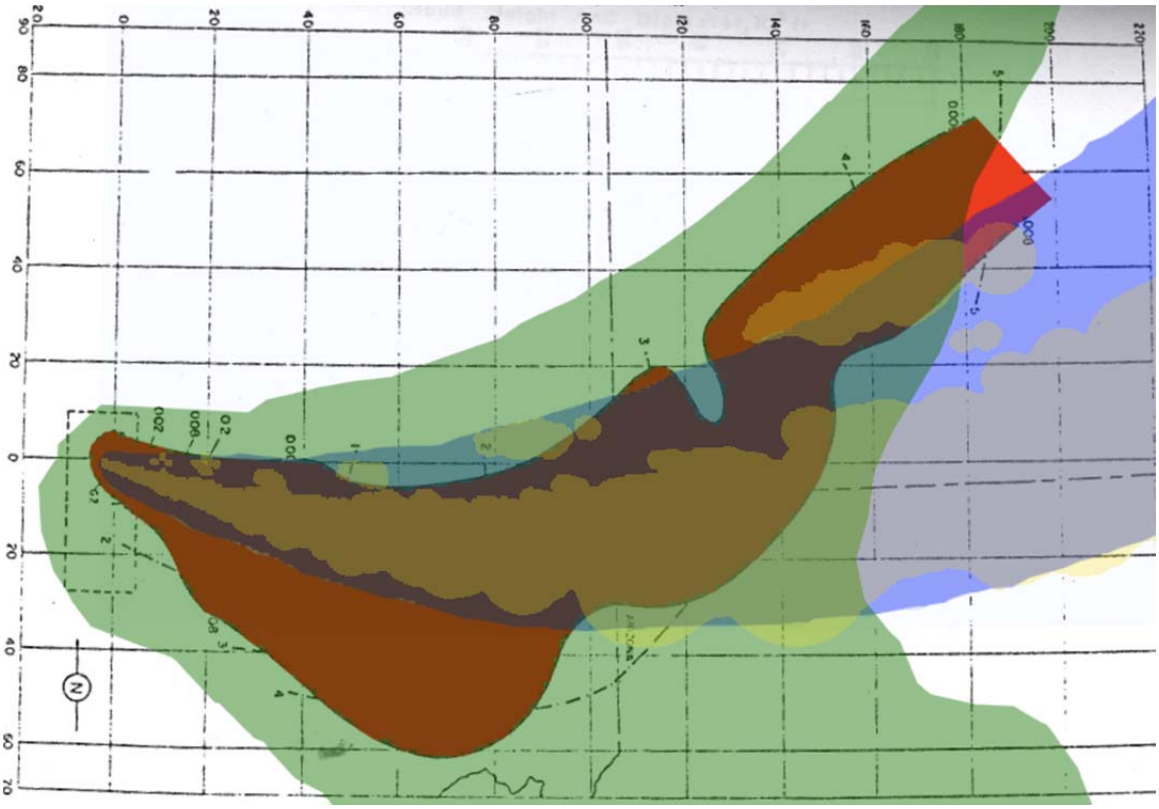

Figure 48. Zucchini Test-Shot 0.008 R/h Dose-Rate Contours: WRF (Green), HPAC (Blue), HYSPLIT (Yellow), and DNA-1251-EX Observational Data (Red)

As seen visually from the fallout patterns in Figure 48 and as reflected in MOE scores shown in Figure 49, both HPAC and HYSPLIT tended to over and under-predict roughly the same amount, with HYSPLIT under-predicting slightly more. This is because the patterns from both models effectively cut the observed patterns at lower dose-rates into halves. The patterns from these two models both over-predicted in the eastward direction and under-predicted in both northward and southward directions.

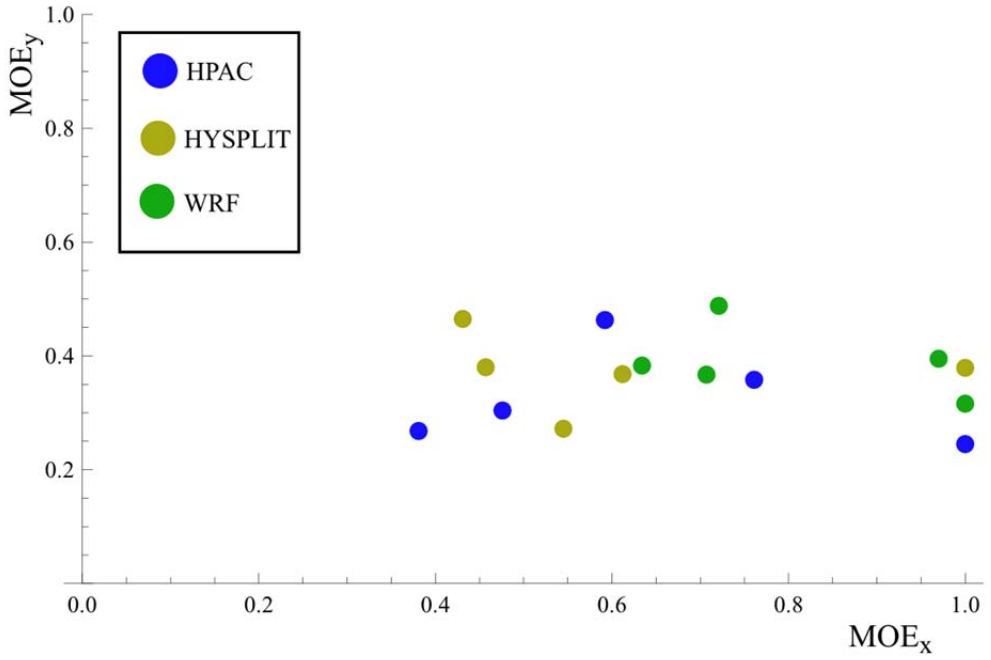

Figure 49. Measure of Effectiveness (MOE) Scores from All Three Models for Test Shot Zucchini

Figure 50Figure 51all three models performed poorly when simulating the Smoky test-shot, with HPAC predicting the most exceptionally inaccurate fallout patterns. The modified WRF model is however the only model that predicts any east-southeastward deposition of early fallout, a fact that gives the model more desirable MOE and NAD scores for the Smoky simulation. All three models describe a general northeast direction of fallout, but all three models fail to transport the particulate far enough east before making the northward turn observed in the DNA-1251-EX pattern after the test detonation.

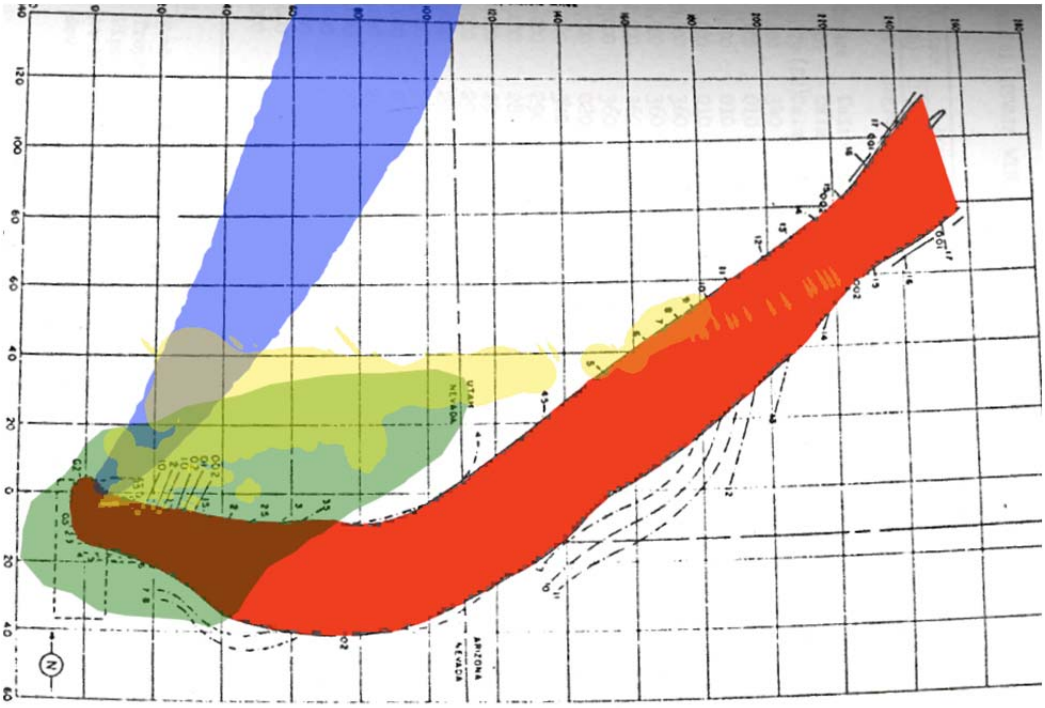

Figure 50. Smoky Test-Shot 0.008 R/h Dose-Rate Contours: WRF (Green), HPAC (Blue), HYSPLIT (Yellow), and DNA-1251-EX Observational Data (Red)

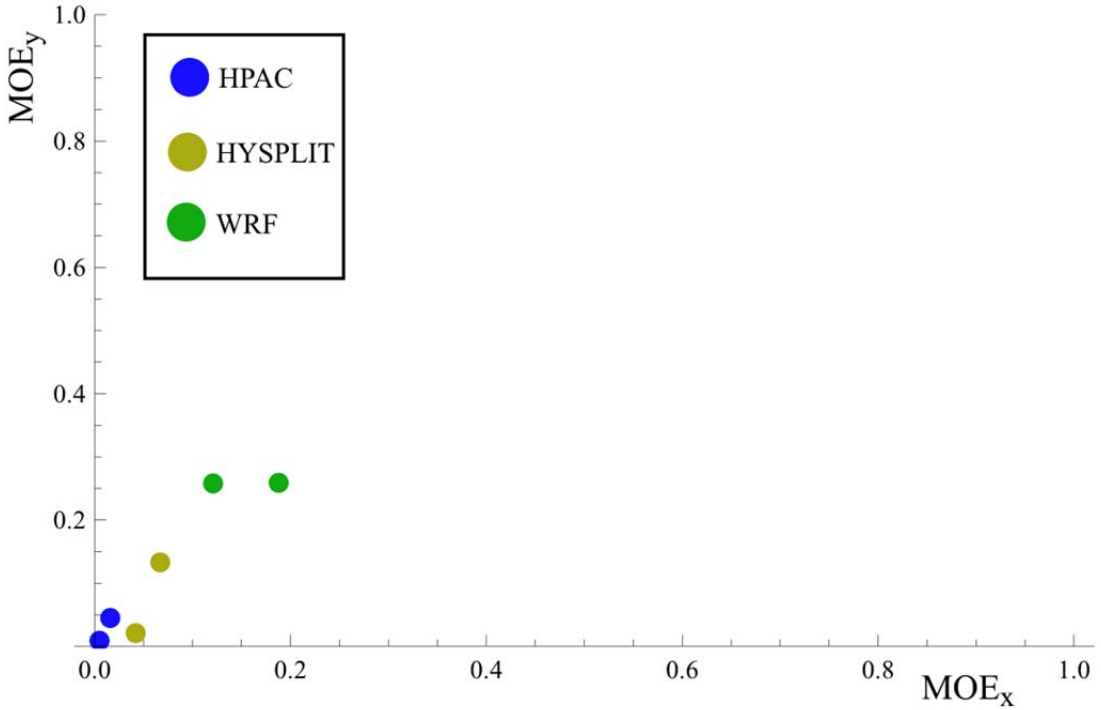

Figure 51. Measure of Effectiveness (MOE) Scores from All Three Models for Test Shot Smoky

5. Conclusions

5.1 WRF/Chem as a Nuclear Fallout Model

The modified WRF/Chem model is not yet ready for use as an operational tool as the currently modified code has significant limitations and certain features that need to be tested. For instance, the code does purportedly have the ability to account for scavenging from rain particulate, but these features and their implications for ultimate fallout accuracy remain untested as there was no rainfall at the Nevada test-sites for the test-shots used as control data for this research. Limitations of the current model include the lack of a cloud-rise algorithm specifically designed for cloud stabilization after an atmospheric nuclear detonation, and the absence of procedures for the insertion of a "hot bubble" for post-detonation weather predictions and feedbacks within the model.

An important finding of this research is that the size distributions of aerosols within the original WRF code are apparently constrained to small sizes (generally less than about 1 μm) and very small terminal velocities (less than about 1 cm/s). The significance of this is that in simulations of atmospheric nuclear detonations that were the focus of this work, the large masses of ejected material are assigned unrealistically slow settling velocities and thus prevented from depositing to the ground in realistic time periods. Only after an algorithm for determining realistic terminal velocities for the larger size distribution was forced into the code were the deposition results shown in Section 4.2 achieved

Given that the modified code as it exists is able to predict fallout somewhat more accurately than the current operational models, the future potential for the code to evolve

into an operational nuclear fallout model can hardly be overstated. Even with its current limitations, the modified WRF model is able to predict historic fallout with generally higher fidelity than both HYSPLIT and HPAC. The measure-of-effectiveness and normalized absolute difference scores numerically verify what is visually observed on the plots of predicted fallout patterns. More intricate elements of the observed fallout patterns are reflected only by the modified WRF model. Perhaps most dramatically, the model is able to predict at least somewhat the direction of early fallout after Operation Plumbbob: Smoky where the other two models completely miscalculate the direction.

5.2 Recommendations for Future Action

Given the potentially enormous consequences that predictions from operational fallout models entail, the need for more capable and more accurate predictions is highlighted by this research. As an approach to this problem, it is recommended that future fallout transport & dispersion (T&D) models be developed such that they are, at their cores, fully functioning numerical weather prediction (NWP) models. This research highlights the potential benefits in terms of accuracy and intricacy of being able to use a wider array of meteorological variables for ingestion into T&D predictions. Given that the long developed Weather Research and Forecasting model is considered the strongest of mesoscale NWP models, and is currently used by many meteorological organizations around the world, and given that the model is open-source and based on mainly Fortran modules, this model is an excellent candidate for modification into what will surely represent a significant step forward for the kinds of fallout forecasting that is so vital to emergency planning personnel.

Furthermore, the development of a WRF-based fallout model, rigorously tested and validated, could represent a clear choice amongst models in terms of desirability. This could lead to the end of scenarios such as that noted after the Fukushima Daiichi nuclear disaster, in which competing models used by various agencies were predicting vastly different fallout patterns, confusing the situation further and throwing evacuation planning into near chaos [from personal communication with Dr. John Mark Maddox of the Defense Threat Reduction Agency, July 2012]. Given that the meteorological community has converged around the WRF model, and given that the root of T&D modeling is weather modeling, it seems reasonable to suggest that the community involved in providing downwind hazard prediction plots might also converge around a WRF-based fallout model, should one be thoroughly developed.

5.3 Recommendations for Future Research

There are many areas in which the research presented can be expanded and improved upon, the most of important of which is developing a method to insert a high temperature sphere into the modified WRF model, either while the model is running, or in the weather data to be used as initial conditions by the model. This will affect the meteorological conditions predicted by the model, which in turn, will affect the deposition of early fallout. This is of critical importance because, as illustrated by the results in the previous chapter, direction of early fallout has a significant impact on determining the overall accuracy of a given prediction. Furthermore, this potential buoyant sphere of high temperatures introduced to the model has the potential, depending on the meteorological conditions of the environment before detonation, to induce rainfall

in the local atmosphere, thus severely changing the area and concentration of activity in the fallout through wet scavenging [1] [11].

Another potential improvement to the modified code as it exists currently would be to re-write the cloud stabilization from its current form into an accurately defined cloud that reflects empirical data concerning nuclear cloud growth. Though the current volcanic ash cloud module, slightly modified to reduce total volume, provides benefits such as the prediction of deposition upwind of ground zero, a module designed specifically for nuclear clouds would surely improve the accuracy of the model. Going beyond the introduction of a stabilized nuclear cloud, a toroidally growing and rising source has been shown to improve fallout predictions [28].

Finally, in order for the modified WRF code to eventually evolve into an operational model, the usability of the model must become simplified. Currently, six executable files must be run separately, each with its own very specific set of text file parameters and intermediate files required for successful execution. Viewing output from the simulation requires writing scripts in NCAR command language and the successful compilation of additional programs and development libraries. The potential exists to package all the separate elements of the program into a single application or executable which, like HPAC, can be used quickly and easily by emergency planning personnel.

Appendix. Compiling WRF/Chem v3.4

Setting up The Weather Research & Forecasting with Chemistry (WRF/Chem) Model onto a new computer can prove challenging since the model depends on many different open-source development libraries, each with their own installation requirements and usage conventions. This appendix presents how WRF/Chem was built for this research with the goal of helping inform future research.

Operating System & Compilers

The WRF/Chem code is currently designed to be compiled to run on either single or multiple Linux computers. For this research the 64-bit Scientific Linux OS 6.2 was used as the operating system. This operating system was developed by the European Organization for Nuclear Research (CERN) and is based off the Red Hat Inc. Enterprise Linux distribution. WRF/Chem can be built onto other Linux operating systems inluding those that are 32-bit, but note that the procedure for installing and compiling WRF/Chem may vary due to differences in how development libraries are stored and shared.

Scientific Linux 6.2 comes with the latest versions of the GNU compilers (gcc, g++, and gfortran) which were employed for building WRF/Chem along with all dependent programs and libraries. When attempting to build the WRF model from source code, it is extremely important that all dependent programs and libraries be built with the same variety of compilers. Fortran95, C, and C++ compilers are required to build and execute WRF/Chem code, and while the software supports the use of many other compilers such as those developed by Intel® and PGI, many of the dependent library packages do not, and it is thus recommended by the researcher that a fresh WRF/Chem build be attempted using GNU compilers first.

Development Libraries

Carefully deciding and keeping track of where dependent libraries and include files should be installed to can prove to be one of the more cumbersome parts of the WRF install process. For simplicity, all development libraries and include files should be installed manually, and from source code, into the same directory. This was done by specifying a "prefix" during the configure stage of each installation. For this research all packages were installed to the /usr directory. This means that all installed include files will be located in the folder "/usr/include" and all libraries will be installed in either "/usr/lib" or "/usr/lib64."

Building WRF/Chem

The Weather Research & Forecasting Model, with or without chemistry, can be built in many different ways depending on any specific file-type compatibility requirements. For example, "GDAL/PROJ.4" support can be included into the WRF build if the user plans on incorporating" shapefile", "mapinfo", or "TIGER" file-types. The vast majority of such proprietary software and file-type support were not needed for this research. Figure 52 shows the basic framework for the model that was installed for this research.

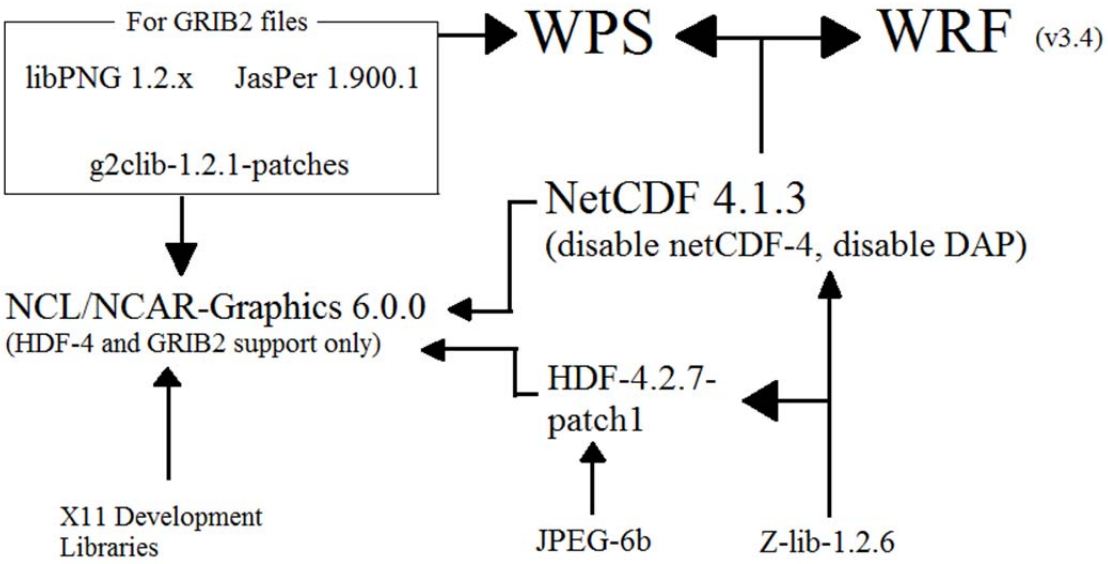

Figure 52. A Schematic of the Dependent Programs and Libraries During WRF Compilation

Important Notes

When attempting to replicate the WRF installation shown above, it is crucial to note that NetCDF-4 was built without "classic" NetCDF-4 support and without OPeNDAP support. This installs what is almost equivalent to NetCDF-3 under the name NetCDF-4 and eliminates the need for a large number of other development libraries including szip, libCurl, and most importantly HDF-5 (v1.8.5-patch1 only) which can be difficult to build correctly from source code.

When installing HDF-4, the location of the Z-lib and JPEG libraries must be specified during the configuration stage. Additionally, "netCDF support" must be disabled and a unique include directory must be specified to ensure that certain NetCDF

include files do not get overwritten. Finally, HDF-4 must be installed before installing NetCDF so that bin commands such as “ncdump” are built by NetCDF and not HDF.

GRIB2 File-type

Most recent gridded meteorological data that can be used for initial and boundary conditions for WRF simulations are in the GRIB2 file format, which was developed by the World Meteorological Organization (WMO). Support for GRIB2 must be built into the WRF installation in order to be able to make real-time forecasts. Thus, if a fully constructed fallout model with a WRF transport & dispersion core is ever to be operationally ready, GRIB2 support should be included.

Bibliography

[1] John W. Englert, *In-Line Particulate Transport and Dispersion Modeling Using The Regional Atmospheric Modeling System (RAMS)*. Wright-Patterson AFB: Air Force Institute of Technology, 2003.

[2] April D. Miller, *A Comparison in the Accuracy of Mapping Muclear Fallout Patterns Using HPAC, HYSPLIT, DELFIC FPT, and an AFIT FORTRAN95 Fallout Deposition*. Wright Patterson AFB: Air Force Institute of Technology, 2011.

[3] Charles J. Bridgman, *Introduction to the Physics of Nuclear Weapon Effects*. Fort Belvoir: Defense Threat Reduction Agency, 2001.

[4] George H. Baker III, *Implications of Atmospheric Test Fallout Data for Nuclear Winter*. Wright-Patterson AFB: Air-Force Institute of Technology, 1987.

[5] Larry W. Burggraf, "Agent Aerosols," Air Force Institute of Technology, Wright-Patterson AFB, Presentation 2010.

[6] Arthur T.A. Hopkins, *A Two Step Method to Treat Variable Winds in Fallout Smearing Codes*. Wright-Patterson AFB: Air Force Institute of Technology, 1982.

[7] Stephen P. Conners, *Aircrew Dose and Engine Dust Ingestion from Nuclear Cloud Penetration*. Wright-Patterson AFB: Air Force Institute of Technology, 1985.

[8] Vincent J. Jodoin, *Nuclear Cloud Rise and Growth*. Wright-Patterson AFB: Air Force Institute of Technology, 1994.

[9] George E. Pugh and Robert J. Galiano, *An Analytical Model of Close-In Deposition of Fallout for Use in Operational Type Studies*. Washington D.C.: The Pentagon, Weapon System Evaluation, 1959.

[10] C.N. Davies, "Definitive Equations for the Fluid Resistance of Spheres," *The Proceedings of the Physical Society Vol. 57*, pp. 259-270, 1945.

[11] A. Barrie Pittock et al., *Environmental Consequences of Nuclear War Volume I: Physical and Atmospheric Effects*, R.E. Munn, Ed. Chichester: John Wiley &

Sons, 1985.

[12] Peter V. Hobbs, *Aerosol-Cloud-Climate Interactions*. San Diego: Academic Press, 1993.

[13] Wanmin Gong, Craig Stroud, and Leiming Zhang, "Cloud Processing of Gases and Aerosols in Air Quality Modeling," *Atmosphere, 2*, pp. 567-616, 2011.

[14] Defense Treat Reduction Agengy (DTRA), *Hazard Prediction and Assessment Capability (HPAC), User Guide, Version 4.04*. Fort Belvoir: Defense Threat Reduction Agency, 2004.

[15] D. Pillai et al., "Comparing Lagrangian and Eulerian models for CO2 transport - a step towards Bayesian inverse modeling using WRF/STILT-VPRM," *Atmospheric Chemistry and Physics Discussions, Volume 12, Issue 1*, pp. 1267-1298, 2012.

[16] Roland R. Draxler and G.D. Hess, "An Overview of the HYPLIT_4 Modeling System for Trajectories, Dispersion, and Deposition," *Austalian Meterological Magazine, 47*, pp. 295-308, 1998.

[17] Air Resources Laboratory. (2012, April) Air Resources Laboratory. [Online]. http://www.arl.noaa.gov/HYSPLIT_info.php

[18] Ashley Francis, "DELFIC: Defense Land Fallout Interprative Code," Air Force Institute of Technology, 2012.

[19] Buckley E. O'Day, *Estimation of Weapon Yield from Inversion of Dose-rate Contours*. Wright-Patterson AFB: Air Force Institute of Technology, 2009.

[20] Jason Knievel, "The WRF Model," in *ATEC Forecasters Conference*, Boulder, 2005, p. 5.

[21] National Center For Atmospheric Research, *Weather Reseach & Forecasting Model ARW Version 3 Modeling System User's Guide*. Boulder, 2012.

[22] J. B. Klemp, W. C. Skamarock, and J. Dudhia, "Conservative Split-Explicit Time Integration Methods for the Compressible," *Monthly Weather Review*, pp. 2897-

2913, August 2007.

[23] William C. Skamarock et al., *A Description of the Advanced Research WRF Version 3*. Boulder: National Center for Atmospheric Research, 2008.

[24] E. Kalnay et al., "The NCEP/NCAR 40-Year Reanalysis Project," *Bulletin of the American Meterological Society*, pp. 437-471, 1996.

[25] Steve Warner, Nathan Platt, and James F. Heagy, "User-Oriented Two-Dimensional Measure of Effectiveness for the Evaluation of Transport and Dispersion Models," *Journal of Applied Meterology Vol. 43*, pp. 58-73, 2004.

[26] R&D Associates, "Characterization of Dust Environments for the F-107, TF-33, and J-57 Engine Tests (U)," Washington D.C., 1988.

[27] Kevin D. Pace, *Terrain and Spatial Effects on a Hazard Prediction and Assessment Capability (HPAC) Software Dose-Rate Contour Plot Predictions as Compared to a Sample of Local Fallout Data From Test Detonations in the Contenental United States, 1945-1962*. Wright-Patterson AFB: Air Force Institute of Technology, 2006.

[28] Karson A. Sandman, *Development of 2-Dimensional Cloud Rise Model To Analyze Initial Nuclear Cloud Rise*. Wright-Patterson AFB: Air Force Institute of Technology, 2005.

REPORT DOCUMENTATION PAGE

Form Approved
OMB No. 074-0188

PLEASE DO NOT RETURN YOUR FORM TO THE ABOVE ADDRESS.

1. REPORT DATE *(DD-MM-YYYY)*	2. REPORT TYPE	3. DATES COVERED *(From – To)*
09-07-2012	Master's Thesis	June 2011 – September 2012

TITLE AND SUBTITLE

Mapping Nuclear Fallout Using The Weather Research & Forecasting (WRF) Model

5a. CONTRACT NUMBER

5b. GRANT NUMBER

5c. PROGRAM ELEMENT NUMBER

6. AUTHOR(S)

Schofield, Joseph C.H., Civilian, USAF

5d. PROJECT NUMBER
If funded, enter ENR #

5e. TASK NUMBER

5f. WORK UNIT NUMBER

7. PERFORMING ORGANIZATION NAMES(S) AND ADDRESS(S)

Air Force Institute of Technology
Graduate School of Engineering and Management (AFIT/ENY)
2950 Hobson Way, Building 640
WPAFB OH 45433-8865

8. PERFORMING ORGANIZATION REPORT NUMBER

AFIT/CWMD/ENP/12-S01

9. SPONSORING/MONITORING AGENCY NAME(S) AND ADDRESS(ES)

High Energy Laser Joint Technology Office (HEL-JTO)
901 University Blvd SE
Albuquerque, NM 87106
(505) 248-8205
Mark.Neice@jto.hpc.mil

10. SPONSOR/MONITOR'S ACRONYM(S)
Fill in

11. SPONSOR/MONITOR'S REPORT NUMBER(S)

12. DISTRIBUTION/AVAILABILITY STATEMENT

APPROVED FOR PUBLIC RELEASE; DISTRIBUTION UNLIMITED.

13. SUPPLEMENTARY NOTES

14. ABSTRACT

There are many models that attempt to predict transport & dispersion (T&D) of particulate matter in the sensible atmosphere. The majority of these existing models are unable to incorporate atmospheric processes such wet deposition through scavenging and cloud condensation nuclei (CCN) formation. To this end, the numerical weather prediction (NWP) model known as the Weather Research & Forecasting with Chemistry (WRF/Chem) Model is studied to determine its suitability as a potential tool for predicting particulate T&D following an atmospheric nuclear detonation. This is done by modifying relevant modules, originally designed to predict the settling of volcanic ash, such that a stabilized cloud of nuclear particulate is initialized within the model. This modified code is then executed for various atmospheric test explosions and the results are qualitatively and quantitatively compared to historical dose-rate contour data contained in DNA-1251-EX. The same simulations were also performed using the offline (NWP wind flow separately applied) Hazard Predication Assessment & Capability (HPAC) Model and Hybrid Single Particle Lagrangian Integrated Trajectory (HYSPLIT) Model. By comparison, using WRF/Chem for particulate tracking allows for the incorporation of important meteorological processes inline with dispersion processes and leads to more realistic fallout pattern with effects of the fallout coupled back into the numerical weather forecast.

15. SUBJECT TERMS

Nuclear fallout modeling, transport & dispersion (T&D) modeling, Weather Research & Forecasting (WRF) modeling, down-wind hazard prediction plots.

16. SECURITY CLASSIFICATION OF:			17. LIMITATION OF ABSTRACT	18. NUMBER OF PAGES	19a. NAME OF RESPONSIBLE PERSON
a. REPORT	b. ABSTRACT	c. THIS PAGE			Steven T. Fiorino, PhD ADVISOR
U	U	U	UU	108	19b. TELEPHONE NUMBER *(Include area code)* (937) 255-6565, ext 4506 (steven.fiorino@afit.edu)

Standard Form 298 (Rev. 8-98)
Prescribed by ANSI Std. Z39-18